Volume 1 | Number 1 | Jan 2013 | Pages 1–100

CrystEngComm

www.rsc.org/crystengcomm

ROYAL SOCIETY OF CHEMISTRY

A table of Contents Entry

Multiscale study of the cationic surfactants influence on amorphous calcium phosphate precipitation

A. Selmani, I. Coha, K. Magdić, B. Čolović, V. Jokanović, S. Šegota, S. Gajović, A. Gajović, D. Jurašin, M. Dutour Sikirić
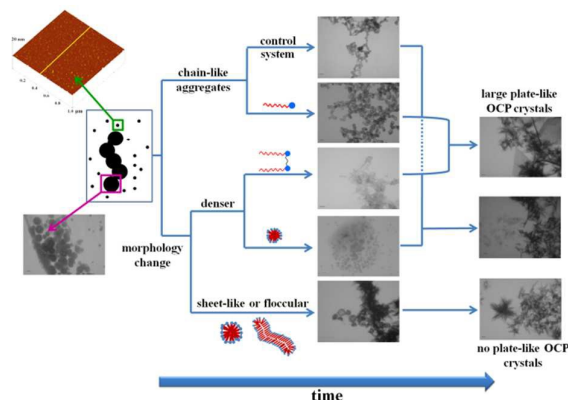
Different effects that surfactant monomers and micelles exert at different length scales during CaPs formation in the solution can lead to similar effects at microscale.

Multiscale study of the cationic surfactants influence on amorphous calcium phosphate precipitation

A. Selmani[1], I. Coha[2], K. Magdić[2], B. Čolović[3], V. Jokanović[3], S. Šegota[2], S. Gajović[4], A. Gajović[5], D. Jurašin[6], M. Dutour Sikirić[6,*]

[1]Department of Chemistry, Faculty of Science, University of Zagreb, Horvatovac 102a, 10000 Zagreb, Croatia
[3]Vinča Institute of Nuclear Sciences, University of Belgrade, Mike Petrovića Alasa 11-14, 11 001 Belgrade, Serbia
[4]Croatian Institute for Brain Research, School of Medicine, University of Zagreb, Šalata 3, 10 000 Zagreb, Croatia
[2]Division for Marine and Environmental Research, [5]Division of Materials Physics and [6]Division of Physical Chemistry, Ruđer Bošković Institute, Bijenička cesta 54, 10 000 Zagreb, Croatia

*corresponding author:

Maja Dutour Sikirić
Laboratory for synthesis and self-assembly processes of organic molecules
Division of Physical Chemistry
Ruđer Bošković Institute
Bijenička cesta 54
10 000 ZagrebCroatia
e-mail: sikiric@irb.hr
Tel: + 385 1 456 0941
http://www.irb.hr/eng/People/Maja-Dutour-Sikiric

ABSTRACT

The influence of monomeric and micellar concentrations of the cationic monomeric, dodecyltrimethylammonium bromide (DTAB) and corresponding dimeric, bis(*N,N*-dimethyl-*N*-dodecyl)ethylene-1,2-diammonium dibromide (12-2-12), surfactants on the formation and transformation of amorphous calcium phosphate (ACP) was investigated. Combination of microscopy (AFM and TEM) and light scattering techniques (size and zeta potential measurements), enabled for the first time, to follow simultaneously the effect that additive exert at different length scales during CaPs formation in the solution - from prenucleation clusters and ACP particles to crystalline phase. Depending on their aggregation state (monomers or micelles) and the geometry of aggregate (spherical or elongated micelles) DTAB and 12-2-12 have exhibited different effects on the rate of ACP transformation, as well as on the morphology of amorphous and crystalline phase. It was shown that the surfactants effect on precipitation process observed at microscale could be a result of different pathways at nanoscale. Obtained results may have implications for understanding general mechanism of inorganic-organic interactions underlying biomineralization processes, as well as for materials science.

INTRODUCTION

Amorphous calcium phosphate (ACP) is the initial solid phase formed during calcium phosphates (CaPs) precipitation from basic and neutral solutions.[1,2] Its excellent biological properties[3] and mounting evidence that its formation is the first step by which hard tissue in vertebrate are formed,[4,5] lately motivates interest for the investigation of ACP formation and its further transformation, as well as for application in different type of biomaterials.[6]

First to propose that formation of ACP is the first step in the precipitation of CaPs was Posner[7] in 1965. Posner also proposed that the basic structural unit of ACP is a spherical cluster $Ca_9(PO_4)_6$, later named Posner's cluster, of about 9.5 Å in diameter.[8] A large number of these clusters are randomly close packed in spheres 30 – 100 nm in diameter, which in turn aggregate into chain-like aggregates.[9,10] Although, existence of Posner's clusters was accepted, only recent development of experimental techniques (cryogenic transmission electron microscopy, cryo-TEM, atomic force microscopy, AFM and dynamic light scattering, DLS) revealed their formation in different experimental conditions.[11-14] However, as it was noted by Dey *et al.*,[13] agreement in size between prenucleation clusters (PNCs) observed in different systems and Posner's clusters should not be taken as a proof of their chemical and structural identity. In the contact with mother liquor ACP is prone to transform into more stable crystalline phase octacalcium phosphate [OCP, $Ca_8(HPO_4)_2(PO_4)_4 \cdot 5H_2O$], calcium hydrogenphosphate dihydrate (DCPD, $CaHPO_4 \cdot 2H_2O$), calcium deficient apatite [CDHA, $Ca_{10-x}(HPO_4)_x(PO_4)_{6-x}(OH)_{2-x}$, $0 < x < 2$] and/or hydroxapatite [HAP, $Ca_{10}(PO_4)_6(OH)_2$].[10,15-18] Therefore, in order to be successfully applied ACP should be stabilized. In organisms ACP is stabilized by specific proteins, like amelogenin and enamelin in teeth.[19] Despite the considerable interest for ACP, the mechanism of its formation and transformation on the nanoscale, as well as role of organic molecules has not yet been fully elucidated.

Surfactants due to their ability to self-assemble in different supramolecular structures and ready availability in many different designs, lend themselves as ideal model systems for systematic studies of the effect of organic molecules on the formation and transformation of ionic crystals.[20] Moreover, they can be used as models even for such a complex systems as proteins and biomembranes.[21] Surfactants typically used for the control of precipitation processes are conventional ones, build of one hydrophilic headgroup and one hydrophobic tail, *i.e.* monomeric surfactants. In the last three decades, dimeric surfactants, consisting of

two molecules of monomeric surfactants covalently linked at the level of the headgroups or close to them with flexible or rigid, hydrophobic or hydrophilic spacer, have drawn considerable attention in both fundamental research and application.[22-25] The reason lies in their superior physicochemical properties in comparison to the corresponding monomeric surfactants. Among dimeric surfactants bisquaternaryammonium surfactants, due to the relative ease of their synthesis and enhanced surface properties, have received much attention. In addition, bisquaternaryammonium surfactants have antibacterial properties and have been used in synthesis of porous materials,[22] making them also of potential interest in the design and preparation of biomaterials. While dimeric surfactants can be found in cosmetic and pharmaceutical products,[25] the investigation of their possible use in controlling precipitation processes are scarce.

The aim of this paper was to assess the influence that monomers and micelles of monomeric dodecyltrimethylammonium bromide (DTAB) and corresponding dimeric bis(*N,N*-dimethyl-*N*-dodecyl)ethylene-1,2-diammonium dibromide (12-2-12) quarternary ammonium surfactant (Scheme 1) exert on the formation and transformation of ACP in solution, in order to contribute to the understanding of the factors governing first stages of CaPs formation in the complex systems. Although, both surfactants have same headgroup(s) and same alkyl chain lengths, connecting two DTAB molecules at the level of headgroups with ethylene spacer results in markedly different 12-2-12 properties. It is known that 12-2-12 is more surface active than DTAB and has peculiar micellization properties.[22,26] Due to the geometric constraints, dimeric surfactants with short ethylen spacer tend, unlike DTAB, to aggregate in elongated and wormlike micelles at relatively low surfactant concentrations even without added electrolyte.[22,26] Such a choice of surfactants enabled assessment of the influence of different surfactant molecular (different number of headgroups and alkyl chains) and aggregate structures (spherical and elongated micelles) on CaPs precipitation while keeping additive chemical functionality and composition the same. The combination of different experimental techniques, microscopy (AFM and TEM) and light scattering techniques (size and zeta potential measurement), enabled for the first time, to follow simultaneously the effect that additive exert at different length scales during CaPs formation in the solution, from PNCs and ACP particles to the final crystalline phase. Understanding interactions in such a complex systems is of interest in materials science for design of new organic-inorganic materials and it also contributes to the understanding of principal factors governing precipitation processes in biological environments.

3
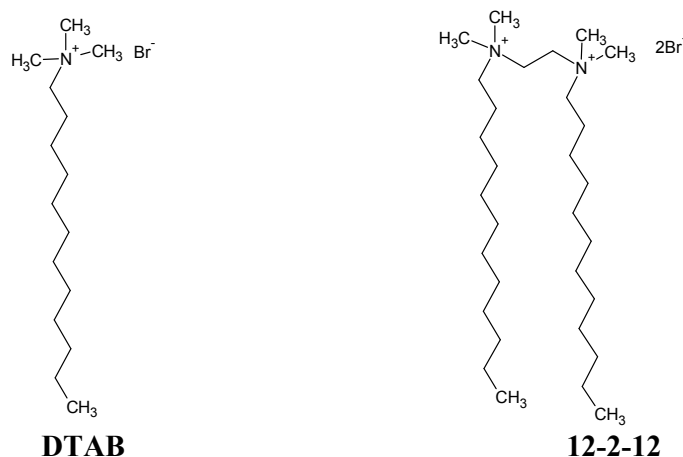
Scheme 1 Molecular structures of monomeric, dodecyltrimethylammonium bromide (DTAB) and its corresponding dimeric, bis(*N,N*-dimethyl-*N*-dodecyl)ethylene-1,2-diammonium dibromide (12-2-12) surfactant.

EXPERIMENTAL SECTION

Materials. Analytical grade chemicals calcium chloride (CaCl$_2$), sodium hydrogenphosphate (Na$_2$HPO$_4$) and dodecyltrimethylammonium bromide (DTAB) were obtained from Sigma Aldrich, Germany. Dimeric surfactant, bis(*N,N*-dimethyl-*N*-dodecyl)ethylene-1,2-diammonium dibromide (12-2-12) was synthesized and characterized as described elsewhere.[24] The purity of surfactants was tested by surface tension measurements, *i.e.* no minima in surface tension isotherm confirmed high purity of both surfactants. MiliQ water (Milipore) was used in all experiments.

CaCl$_2$ and Na$_2$HPO$_4$ stock solutions were prepared from analytical grade chemicals which were dried overnight in a desiccator over silica gel. The pH of sodium hydrogenphosphate stock solution was adjusted to 7.4 with HCl. Each stock solution contained 0.05% sodium azide to prevent bacterial contamination. Stock solutions of DTAB and 12-2-12 were prepared by weighting dried surfactants and their dissolution in water.

Surfactant/Na$_2$HPO$_4$ systems. The presence of electrolyte can significantly alter interfacial and micellization properties of ionic surfactants.[27] Therefore, in order to determine monomer and micellar surfactant concentrations in given experimental conditions, DTAB and 12-2-12 solutions at electrolyte concentration corresponding to the one in precipitation system, c(Na$_2$HPO$_4$) = 3 mmol dm^{-3} and pH = 7.4 were prepared for surface tension measurements (for the details of surface tension measurement please see Methods section).

4

Preparation of precipitation systems. Control precipitation system was prepared by fast mixing of equal volumes of equimolar $CaCl_2$ and Na_2HPO_4 solutions. Anionic and cationic reactant solutions used for precipitation experiments were diluted from the respective stock solution. The initial concentrations in precipitation system were $c(CaCl_2) = c(Na_2HPO_4) = 3 \cdot 10^{-3}$ mol dm^{-3} at pH = 7.4. In the control system resulting saturation indices of HAP, OCP and ACP were 13.5, 5.2 and 3.7, respectively. Precipitation systems containing surfactants monomer and micellar concentrations were prepared by adding respective surfactant solutions to phosphate solution before mixing reactant solutions and readjusting pH if necessary. Surfactant concentrations for precipitation systems below and above corresponding cmc, as well as, in case of 12-2-12, above 2nd break observed in surface tension isotherm were chosen. In that way, investigation of the influence of surfactant monomers and different micellar structures on ACP formation and transformation was possible. Solution composition of investigated precipitation systems is given in Table 1.

Table 1 Solution composition of investigated precipitation systems. $pH_{init} = 7.4$, θ / °C = (25 ±0.1).

system	$c(CaCl_2)$ / mmol dm^{-3}	$c(Na_2HPO_4)$ / mmol dm^{-3}	$c(DTAB)$ / mmol dm^{-3}	$c(12\text{-}2\text{-}12)$ / mmol dm^{-3}	
CS	3	3			
MS1	3	3	0.1		monomers
MS2	3	3	30		micelles
DS1	3	3		0.01	monomers
DS2	3	3		0.5	micelles
DS3	3	3		3	micelles

CS – control system, MS – monomeric surfactant, DS – dimeric surfactant

The precipitation experiments were performed at 25 ± 0.1 °C without additional stirring. The precipitation of calcium phosphate was followed by continuously monitoring pH changes (Metrohm 701 pH/Ion meter). Samples for further analysis were taken after 10 and 30 minutes, as well as after 24 hours aging time. These time periods were chosen based on pH measurements, to enable precipitate characterization at different precipitation stages.

Methods

Surface tension measurements. The surface tension (γ) of surfactant solutions containing Na$_2$HPO$_4$ ($c = 3 \cdot 10^{-3}$ mol dm^{-3}) at pH = 7.4 was measured using the Du Noüy ring method (Interfacial Tensiometer K100, Krüss, Germany). The γ was measured to within 0.001 mN m^{-1}. These values were then corrected by using the tables of Huh and Mason. The surface tension of water was measured regularly in order to provide values for the pure solvent and to check that the technique was being properly carried out. All measurements were conducted at 25 ± 0.1 °C.

The size distribution and zeta potential of surfactant micelles and CaPs particles was determined by means of dynamic light scattering using a photon correlator spectrophotometer equipped with a 532 nm "green" laser (Zetasizer Nano ZS, Malvern Instruments, UK). Intensity of scattered light was detected at the angle of 173°. The measurements were performed without filtering the samples, to avoid perturbations. In a polydisperse sample, the scattering from larger particles dominates the scattering from smaller particles, *i.e.* intensity-weighted size distributions obtained by DLS overestimate larger particles. To avoid overestimation arising from the scattering of larger particles, the hydrodynamic diameter (d_h) was obtained as a value at peak maximum of size volume distribution function. Each sample was measured 5 times and the results were expressed as the average value. Although, the precipitated particles were not expected to be only spherical, the determined d_h could considered to be a characteristic size[28] and as such was used in previous studies of calcium phosphate precipitation.[28-30] The zeta potential (ζ) was calculated from the measured electrophoretic mobility by means of the Henry equation using the Smoluchowski approximation. The data processing was done by Zetasizer software 6.32 (Malvern instruments). All measurements were conducted at 25 ± 0.1 °C.

Atomic force microscopy. The samples for AFM imaging were prepared by deposition of sample drop on the substrate surface. Hydrophilic fresh cleaved mica, attached to the metal disc, was used as substrate for the deposition of the 5 μl of suspensions and used for the AFM imaging. After appropriate time of the deposition, the surfaces were washed with MilliQ water 3 times to remove excess surfactant. Prior to the AFM imaging the surface of the samples was additional dried in the stream of nitrogen and left to dry. The morphology of the smallest precipitated particle structures, *i.e.* PNCs, was determined using a MultiMode Probe Microscope with a Nanoscope IIIa controller and a "J" scanner with a vertical engagement (JV) 125 μm (Veeco Instruments, Bruker, Santa Barbara, CA). Tapping mode imaging was

performed under ambient conditions in air using a silicon tip (TESP, Veeco, nom. freq. 320 kHz, nom. spring constant 42 N/m). The linear scanning rate was optimized between 1.0 and 1.5 Hz at the scan angle 0°. Images were processed and analyzed by means of the offline AFM NanoScope software, version 5.12r5. Particle dimensions of the granular microstructures were determined by means of the Particle Analysis option within the AFM software.

Transmission electron microscopy and selected area electron diffraction. Transmission electron microscopy images were obtained using TEM 902A Zeiss (Oberkochen, Germany) operated at 80 kV. For TEM/SAED analysis the drop of suspension was placed on the copper grid covered with Formvar membrane. Excess solution was removed by filter paper and the precipitate was washed three times with drop of MiliQ water. After removing excess water, samples were dried in the stream of nitrogen and kept in desiccator until further analysis. Particle size distributions from TEM micrographs were determined by image analysis program ImageJ 1.48v (freely available at http://imagej.nih.gov/ij/). At least 20 – 80 particles were measured for each sample.

Fourier Transform Infrared Spectroscopy. For FTIR characterization precipitates were filtered through 0.1 μm Milipore filter, washed 3 times with MiliQ water, ethanol and dried in the stream of nitrogen. A small amount of precipitate was finely ground with KBr and the mixture was pressed into pellets by using hydraulic press. FTIR spectra of prepared KBr pellets were recorded on ABB Bomem MB102 FTIR spectrophotometer from 4000 – 400 cm^{-1}, with resolution 2 cm^{-1}. The spectra are average of, 32 scans.

Powder X-ray diffraction (XRD). For powder XRD characterization samples were centrifuged at 6000 rps (Hettich EBA 8), washed 3 times with water, once with ethanol and vacuum dried. Powder XRD patterns were obtained by an *ItalStructures* diffractometer APD 2000 using CuK$_\alpha$ radiation (graphite monochromator). XRD patterns were scanned in 0.04^o steps (2θ) in the 2θ range from 3.25^o to 60°. The obtained powder patterns were compared with the reference patterns for OCP (ICCD #01-074-1301), HAP (ICDD #01-082-1943), and DCPD (JCPDS #09-0077).

Data interpretation

The maximum surface excess of surfactant molecules (Γ_{max}) at the air/solution interface was calculated from the maximal slope (dγ/dlog *c*) in the surface tension *vs.* concentration curve using Gibbs adsorption equation:[27]

$$\Gamma_{max} = -\frac{1}{2.303nRT}\left(\frac{\partial\gamma}{\partial\log c}\right)_T \qquad (1)$$

where R is gas constant and T temperature. The prefactor n, which is theoretically dependent on surfactant type, in the presence of a swamping electrolyte equals 1. The minimum area (a_{min}) occupied by a surfactant molecule at the air/solution interface can be evaluated from Γ_{max}:

$$a_{min} = \frac{10^{18}}{N_A \Gamma_{max}} \qquad (2)$$

where Γ_{max} is in mol m^{-2}, a_{min} is in nm^2 and N_A is Avogadro's number.[27]

Values of the critical micelle concentration (cmc) were determined from the intersection of the two straight lines drawn in low and high concentration regions in surface tension curves (γ vs. log c) using a linear regression analysis.

The ion activities in the control precipitation system were calculated by VMINTEQ 3.0 (freely available at http://vminteq.lwr.kth.se/download/). Activity coefficients were calculated using Davies approximation of Debye-Hückel equation ($b = 0.3$). Saturation index (SI) defined as:

$$SI = \log IAP - \log K_{sp} \qquad (3)$$

where IAP is actual ion activity product and K_{sp} is solubility product for a given phase, was calculated using solubility products available on MINTEQ database within the software.

RESULTS AND DISSCUSION

Properties of surfactant/Na$_2$HPO$_4$ systems.

It is well established that the presence of an electrolyte in an aqueous solution of ionic surfactant can significantly alter its interfacial and micellization behavior due to screening of the ionic headgroups charge. As a result, the electrostatic repulsions between surfactants headgroups within the adsorbed monolayer and micelles are reduced.[27] Therefore, DTAB and 12-2-12 interfacial and micellization properties were determined in the presence of actual phosphate concentration in precipitation system. Detailed description and discussion of the obtained results are given in ESI. Here brief description of main findings is presented.

Surface tension and dynamic light scattering measurements revealed the difference in DTAB and 12-2-12 interfacial and micellization properties (Fig. S2 and S3†, Table 2). As expected,[22,24] 12-2-12 was more efficient in lowering surface tension and had much lower

cmc in comparison with DTAB (Fig. S2†, Table 2). In addition, 12-2-12 molecule occupied larger area at air/solution interface than DTAB.

The difference in micellization behavior indicated by the shape of surface tension isotherms of DTAB and 12-2-12 was confirmed by DLS and zeta potential measurements. At concentration above cmc, only small DTAB micelles with average hydrodynamic diameter of 3.6 ± 0.3 nm (Fig. S3a†) and ζ potential of 29.6 ± 2.5 mV, were detected. Unlike DTAB, DLS measurements revealed that the value of hydrodynamic diameter of the 12-2-12 micelles increased with increasing surfactant concentration from 4.7 ± 0.5 nm immediately above cmc to 10.9 ± 0.4 nm at concentrations above 2nd break in surface tension isotherm (Fig, S3b†). In addition, at concentrations above 2nd break, a bimodal distribution of 12-2-12 micelles ζ potential was observed (peaks at 14.2 ± 4.8 and 37.7 ± 7.3 mV). Based on these results and literature data for DTAB[22,24,31] and 12-2-12[22,32] it is reasonable to assume the existence of spherical micelles in investigated DTAB system and 12-2-12 system in concentrations immediately above cmc, and coexistence of spherical and elongated micelles at 12-2-12 concentrations above 2nd break.

Table 2 Maximum surface excess concentration (Γ_{max}), minimum area per surfactant molecule (a_{min}) and critical micelle concentration (cmc) obtained from surface tension measurements for monomeric DTAB and dimeric 12-2-12 surfactant in the presence of electrolyte, $c(Na_2HPO_4) = 3 \cdot 10^{-3}$ mol dm^{-3}. pH$_{init}$ = 7.4, θ / °C = (25 ±0.1).

surfactant	Γ_{max}[a]/ mol m^{-2}	a_{min}[a] / nm^2	cmc / mmol dm^{-3}
DTAB	1.93	0.86	14.6
12-2-12	0.96 (1.9)	1.74 (0.87)	0.36

[a]Values in the brackets are expressed per alkyl chain in the molecule of dimeric surfactant.

Based on these results, surfactant concentrations for the precipitation experiments were chosen (Table 1) below (MS1 and DS1) and above (MS2 and DS2) corresponding cmc values, as well as above the second break (DS3) observed in the surface tension *vs.* concentration curve of 12-2-12 (Fig. S2b†). In that way, it was possible to assess how different charge and rigidity of monomers molecule, as well as the different charge density and distribution, size, shape and curvature of micelles affected ACP formation and transformation. It should be noted, that in micellar surfactant solutions, monomers and micelles coexist in dynamic equilibrium.[27]

9

The influence of monomeric and dimeric surfactants on the ACP precipitation

As Bleek and Taubert have recently pointed out, different investigations of the influence of the additives on CaPs formation and transformation are done in a wide range of experimental conditions and therefore their results cannot be fully compared.[33] In order to be able to compare the results obtained in this study with literature data to a larger extent, conditions corresponding to the study of anionic and cationic polyelectrolytes (PEs) influence on ACP formation (Bar-Yosef *et al.*[10]) were chosen. The choice was motivated by parallels that can be drawn between behavior of PEs and surfactants in precipitation systems. Unlike small molecular additives, surfactants included, PEs can, depending on their solution concentration, exhibit dual role in precipitation process, *i.e.* they can act as a promoters or as an inhibitors. Explanation for such a behavior is that at low concentrations polyelectrolytes can act as heterogeneous nucleation centers, while at high concentrations they can inhibit the growth of nascent nuclei.[20] Studies of surfactant influence on the formation of different biominerals (CaPs, calcium oxalates and carbonates) have shown that surfactant micelles can act as a template for the formation of solid phase, facilitating nucleation and/or initial growth.[20] In addition, as an explanation for the observed changes in the crystallizing polymorph or crystal hydrate, a preferential adsorption of the surfactants on the nuclei of one phase was suggested as a possible mechanism.[20] The mode of adsorption, consequently the effect on nascent solid phase, of PEs[10] as well as of surfactants[34,35] depends on their concentration and molecular structure.

The influence of monomeric and dimeric surfactants on the rate of ACP transformation

Precipitation of CaPs is followed by changes in pH which enables to follow advancement of the reaction, at least (semi)qualitatively, by monitoring pH of the precipitation system. In Fig. 1, the results of the free drift experiments are shown. Since pH in stage 2a remained relatively stable during first 15 minutes, this pH value was fixed the same for all systems in order to be able to compare surfactants influence on nucleation kinetics. The raw data are presented in Fig. S4†. As it can be seen the process can be divided in several stages. In all systems in the first stage (section 1, Fig. 1) pH dropped immediately upon mixing reactant solutions, followed by its gradual increase. The initial pH drop can be ascribed to ion pair formation.[30,36] Since pH of the system is a function of $H_2PO_4^-/HPO_4^{2-}$ molar ratio, comparing its value before mixing reactant solutions with the

10
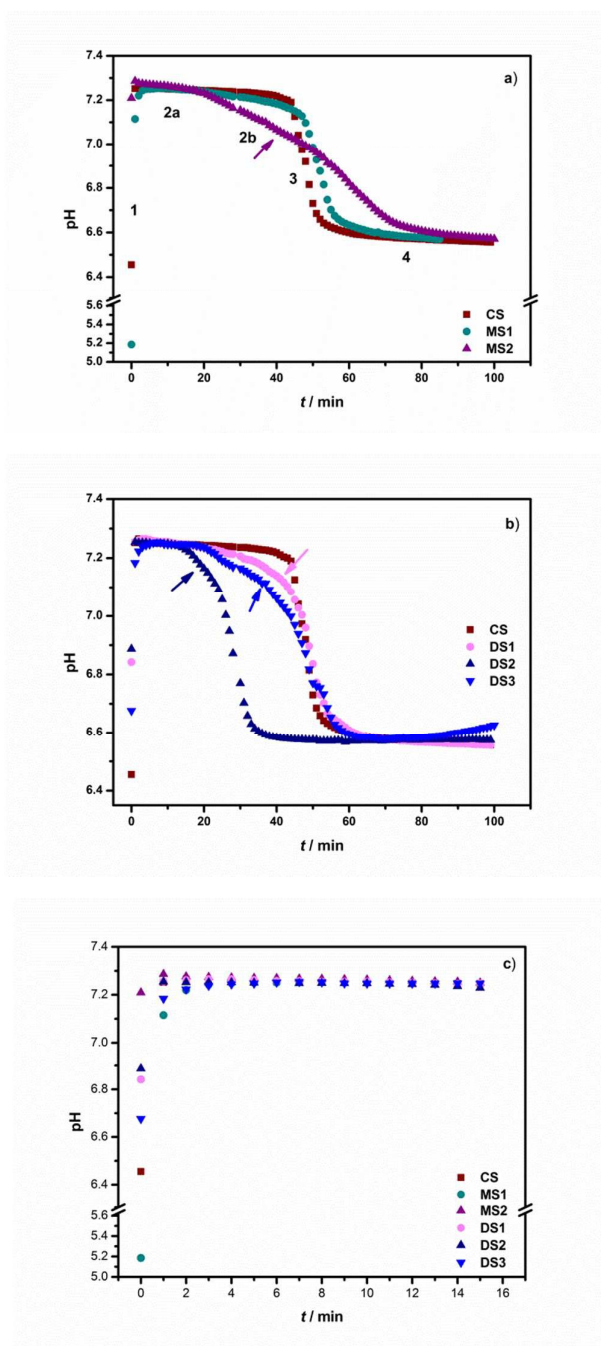
Fig. 1 Representative pH *vs.* time curve of amorphous calcium phosphate (ACP) formation and transformation in the absence (CS) and presence of monomer and micellar concentrations of a) DTAB (MS1 and MS2) and b) 12-2-12 (DS1, DS2 and DS3). c) pH change in the first 15 minutes of precipitation process. Since pH in stage 2a remained relatively stable during first 15 minutes, this pH value was fixed the same for all systems for the comparison of surfactants influence on nucleation kinetics. $pH_{init} = 7.4$, θ / °C = 25 ± 0.1. Different precipitation stages are marked (1-4). Arrows denote section 2b.

11

value of the molar ratio $CaH_2PO_4^+ / CaHPO_4$ after mixing, can be used to corroborate the assumption of ion pair formation, as described by Wang *et al.*[30] In our experimental conditions molar ratio $H_2PO_4^-/HPO_4^{2-}$ can be calculated as $H_2PO_4^-/HPO_4^{2-} = 10^{-pH}/K_{a2}$[30], which at pH 7.4 and 25 °C equals 0.64 ($K_{a2} = 6.2 \cdot 10^{-8}$)[37]. Using concentrations calculated with VMINTEQ 3.0, it turns out that the molar ratio $CaH_2PO_4^+ / CaHPO_4$ is lower than molar ratio $H_2PO_4^- / HPO_4^{2-}$ (0.035 : 0.64) and as a result pH decreased. Subsequent pH increase, previously explained with the formation of ion clusters,[30,36] was followed by the stage in which pH slightly decreased (section 2a, Fig. 1a). This stage is associated with the formation of ACP, during which the changes in pH and calcium concentrations are small or absent.[10,16,30,36,38] As it can be seen from Fig. 1c, except in the presence of DTAB monomers (MS1) the initial pH drop in systems containing surfactants is smaller than in control system. Studies of cethyltrimethylammonium bromide surface and micellization properties in the presence of PO_4^{3-} ions have shown that phosphate ions can exchange bromide ions on the surface of the micelle.[39] Based on this result it could be assumed that phosphate ions bind to DTAB and 12-2-12 micelles surface in investigated systems, in that way influencing the initial pH change. However, due to the lack of the relevant equilibrium data for the micelles/phosphate systems, it is not possible to quantify this influence following Wang *et al.*[30] approach for control system. The explanation of pH changes in precipitation systems containing monomers is not straightforward and needs more investigation of DTAB and 12-2-12 monomers interaction with phosphate ions. In DTAB and 12-2-12 solutions at surfactant concentrations below cmc, both monomers are considered to be fully dissociated[22], which cannot account for the observed changes in initial pH. The slopes of the section 2a of pH curves did not differ much, indicating similar rates of ACP formation in all systems.

In control system and MS1, stage 2a is followed by abrupt decrease in pH of the system as a consequence of deprotonation of $H_2PO_4^-$ and HPO_4^{2-} ions associated with the formation of mineral precipitates,[38] *i.e.* secondary precipitation of crystalline phase upon ACP (section 3, Fig. 1a). However, in the precipitation system containing micellar DTAB solution (MS2) and in the systems with 12-2-12 as additive (DS1, DS2 and DS3) between section 2a and abrupt decrease in pH (section 3), a region was detected in which gradual decrease in pH occurred (section 2b, Fig. 1a,b), indicating difference in pathway of ACP/crystalline phase transformation as compared to control system and MS1.[17,40]

Abrupt pH decrease in section 3 of pH curve is associated with the secondary precipitation of crystalline phase upon ACP.[10,38] Unlike in other systems, drop of pH in section 3 in MS2 system is slow. Similar behavior was observed in the studies of ACP mediated HAP nucleation kinetics[41] and ACP stabilization by citrate.[42] This slow change of pH in is attributed to reduced rate of ACP transformation.[30] In the final stage solution mediated growth and phase transformation occurs (section 4, Fig. 1), followed by slight pH change.[10,38]

Recent studies of different additives (amino acids (Asp, Lys, Gly)[43], magnesium[36,43] and citrate[42] ions, phosphorylated osteopontin peptides[38], cationic and anionic PEs[10]) influence on ACP formation and transformation showed that in their presence mineralization pathway remains the same as compared to the control. While interactions of small molecular additives and ions with nascent solid phase are dominated by electrostatic forces, surfactants adsorption behavior is governed by two opposing interactions, electrostatic and hydrophobic, which could be the origin of their more complex role in the precipitation process. 12-2-12 monomers not only have higher positive charge than DTAB monomers (in the solutions 12-2-12 monomers are considered to be fully dissociated[22]), but the presence of two alkyl chains affects the hydrophobic interactions during adsorption. As a consequence 12-2-12 monomers exhibit stronger influence on the precipitation processes than DTAB at much lower concentrations, resulting in effect similar to the DTAB and 12-2-12 micelles.

The different rate of pH change in the stages of ACP and crystalline phase formation allows determining the induction time for nucleation of crystalline phase (t_i), from intersection of the tangents drawn on the second and third section of pH *vs.* time curve.[10,42] For MS2, DS1, DS2 and DS3 systems, intersection of tangents drawn on sections 2b and 3 of pH curve was used to calculate t_i. The induction time is frequently used as an indicator of ACP stability, *i.e.* the longer it is, more stable ACP is considered to be.[10,42]

The induction time, obtained from the free drift experiments, depended both on the surfactant concentration and structure of the micelles (Table 3). Monomer concentrations of both surfactants, as well as micellar DTAB concentration have negligible effect on induction time. However, the induction time is significantly shorter in the presence of 12-2-12 micelles, with more prominent effect observed in the presence of smaller, spherical micelles (DS2). Considering the importance of electrostatic forces in precipitate/additive interactions,[20,33] it seems that the difference in the overall charge of monomer and micelles and charge distribution at the micelle/solution interface could be the origin of the observed effects.

Surfactant monomers have lower charge in comparison with their aggregates and therefore it can be expected that they influence t_i to a much smaller extent.

Table 3. Average induction times (t_i) obtained from pH *vs.* time (t) curves (Fig. 1) from 5 measurements with standard deviations (SD). $pH_{init} = 7.4$, θ / °C = (25 ±0.1).

system	t_i / min	SD
CS	45.2	1.8
MS1	46.1	5.2
MS2	43.8	4.1
DS1	43.3	3.6
DS2	22.8	1.6
DS3	34.9	5.1

Influence of DTAB (MS2) and 12-2-12 (DS2 and DS3) micelles on t_i was very different. Small, spherical DTAB micelles didn't affect t_i at all, while, somewhat larger, spherical 12-2-12 micelles were the most effective in promoting ACP/crystalline transformation (the shortest t_i). The DTAB and 12-2-12 micelles not only have different size and ζ potential (as described in previous section), but it is also known that they have different distribution of headgroups distances at the micelle/solution interface, *i.e.* different charge distribution. The distribution of the headgroup distances at DTAB micelle/solution interface is monomodal peaked at a thermodynamic equilibrium distance determined by the opposite forces at play in micelle formation.[22,26] On the other hand, in the case of 12-2-12 micelles, distribution is bimodal, with additional peak at the distance corresponding to the fully extended ethylene spacer.[22,26] Micelles are not rigid structures and it can be expected that they can adapt to a certain extent to the ionic structure of the nascent solid, *i.e.* act as efficient promoter of crystalline phase formation. The observed difference in t_i between spherical DTAB (MS2) and 12-2-12 micelles (DS2) could mean that bimodal charge distribution enabled 12-2-12 micelles to more easily adapt to the structure of crystalline CaP. The 12-2-12 spherical micelles (DS2) are also more effective than 12-2-12 elongated micelles (DS3) in reducing t_i. Although, charge distribution at the micelle/solution interface is bimodal for both types of micelles, in general, elongated micelles have lower surface charge density than spherical[22] and therefore exhibited less pronounced effect on t_i. In support of this conclusion is observation that present at low concentrations, poly-L-lysine (PLL), poly-L-glutamic acid (PGA) and polystyrene sulfonate (PSS) promote ACP transformation, with high molecular weight polyelectrolytes being more effective in decreasing t_i than low molecular weight,

14

probably due to higher number of the charged group present in the molecule.[10] However, when discussing influence of polyelectrolytes molecular weight, it should be taken into account that PEs with different molecular weight can adopt different conformations. High molecular weight PE can adopt less flexible conformation and/or conformation in which not all functional groups are available for interaction with solid phase. As a result the effect of high molecular weight PE can be less strong than the one of low molecular weight PE, *e.g.* like in case of poly(acrylic acid).[44]

To reveal the nature of processes observed in pH curves, samples collected after 10 and 30 minutes, as well as after 24 hours aging time were subjected to further analysis.

The influence of monomeric and dimeric surfactants on the properties of amorphous phase

Mechanism of CaPs formation and transformation is a complex one, in which processes take place simultaneously at different length scales. Even when using state-of-art techniques, characterization of polydispersed systems, especially the ones containing particles of significantly different sizes, still represents a challenge. Having this in mind, in this study we have combined microscopic techniques (AFM and TEM) with DLS. An important advantage of AFM and TEM is that imagining and analysis of the smallest nanoparticles can be achieved. In addition, AFM and TEM can provide reasonably accurate number average dimension, but the number of analyzed particles is relatively low. This makes it difficult to obtain representative statistics.[45] On the other hand, representative statistics can be obtained by DLS since the amount of sample and consequently number of particles analyzed is much larger than with AFM and TEM. In addition, DLS is a widely used technique for determination of the size of nanoparticle aggregates in suspensions. But since the intensity of light scatter of particles varies with the 6th power of particle radius, the contribution of larger particles can be overestimated or signal of smaller particles can be masked.[45,46] Therefore, in this study the size and morphology of PNCs were determined by AFM imagining. The size and morphology of ACP spherical particles was deduced from TEM micrographs, while the size distribution of their aggregates was measured by DLS.

Precipitation systems after 10 min aging time. In the control system, after 10 min reaction time, AFM and TEM micrographs revealed coexistence of the PNCs (Fig. 2a), spherical ACP particles and chain-like aggregates of spherical particles (Fig. 3a). The corresponding FTIR spectra (Fig. S5†) showed phosphate and hydroxyl bands characteristic for amorphous calcium phosphate.[6]
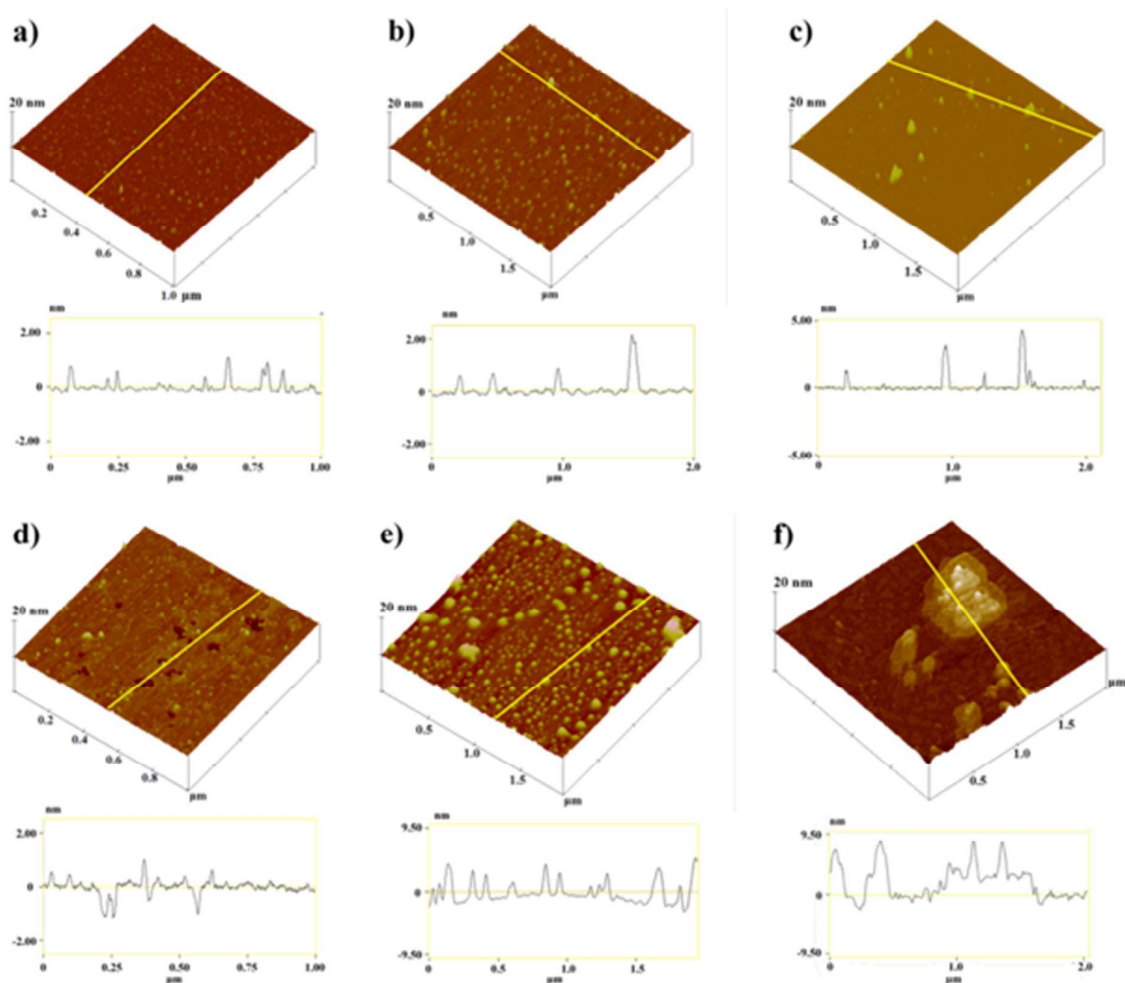
Fig. 2 Atomic force microscopy 3D topographic views (top) and section profiles (bottom) of the particles formed in the systems a) without (CS) and (b-f) in the presence of surfactants: b) DTAB monomers (MS1), c) DTAB micelles (MS2), d) 12-2-12 monomers (DS1), e) 12-2-12 spherical (DS2) and f) 12-2-12 elongated micelles (DS3) after 10 minutes aging time. pH_{init} = 7.4, θ / °C = (25 ±0.1). All samples are presented on 2 μm × 2 μm surface areas with vertical scales 20 nm.

Average height of small particles in the control system (height ~ 1.4 nm), imaged by AFM, was attributed to PNCs (Table 4). Previous studies have shown that the size of PNCs can vary depending on the supersaturation, pH and the presence of the template. Clusters with size in range 0.70-1.00 nm were detected in SBF by DLS.[11] This was confirmed by cryo-TEM[13] which has shown that isolated PNCs with average size 0.87±0.2 nm form in SBF. In the presence of amelogenin clusters of ~ 1nm were observed by TEM.[29] Additionaly, cryo-TEM and TEM studies revealed that PNCs can exist as polymeric assemblies.[13] [,29,40] According to prenucleation clusters definition by Gebauer et al.[47] PNCs are solutes without an interface and therefore there is no driving force for their aggregation. This means that only

16

discrete, non-aggregated, clusters can be considered to be PNCs. On the other hand, clusters that form polymeric assemblies have interfacial surface which drives aggregation and should be considered to be nanophase.[47] Distribution of PNCs sizes was asymmetric with a small population of cluster with larger sizes (up to 4.7 nm). Similarly, asymmetric size distribution of calcium carbonate clusters with majority of particles in the range from 0.6 to 1.1 nm and a small population of larger clusters (up to 4.5 nm) was observed with cryo-TEM.[48] The presence of larger nanoclusters was ascribed to the onset of aggregation process leading to nucleation.[48]

Table 4 Average height, its standard deviation (SD), height minimum (min) and maximum (max) values, of the prenucleation clusters formed in the systems without and in the presence of surfactants) after 10

and 30 minutes aging time measured by atomic force microscopy (AFM). pH_{init} = 7.4, θ / °C = (25 ±0.1).

t	10 min				30 min			
system	height/nm	SD	min / nm	max / nm	height/nm	SD	min / nm	max / nm
CS	1.4	0.3	1.0	4.7	1.0	0.1	0.8	1.1
MS1	1.0	0.3	0.6	3.1	1.1	0.2	0.8	2.0
MS2	1.2	0.9	0.6	6.2	2.2	1.0	1.6	12.7
DS1	1.4	0.4	1.0	7.4	0.7	0.3	0.4	1.4
DS2	1.5	0.6	1.0	4.3	2.7	1.3	1.0	8.0
DS3	2.0	0.8	1.6	7.1	2.7	0.8	2.0	6.8

Control system (CS), DTAB monomers (MS1), DTAB micelles (MS2), 12-2-12 monomers (DS1), 12-2-12 spherical (DS2) and 12-2-12 elongated micelles (DS3)

Due to the small amount of sample used for AFM imagining, it was possible that, although present, polymeric assemblies of nanoclusters were not detected. Therefore the DLS was used to verify AFM data. Larger ACP particles were removed from control system after 10 and 30 min aging time by centrifugation. PNCs and polymeric assemblies were not detected after 10 min, probably due to low concentration. However, after 30 min aging time particles of sizes ranging from around 1.3 nm to several hundred nms were detected. Below 20 nm, particles in size categories of around 1.5 nm, 5.6 nm, 10 nm and 15 nm were detected, confirming both existence of individual PNCs and polymeric assemblies of CaPs clusters (Fig. S7†).

Spherical ACP particles formed in the control system after 10 min have an average size of 127± 55.8 nm as measured from TEM micrographs (Fig. 3a, Table 5), similar to the sizes reported in the other studies.[10,15,20] The size distribution of spherical particles was broad indicating polydispersed sample (Figure S9a†). Information about extent of their aggregation

17

was obtained from the volume size distribution measured by DLS (Figure S10a†) which showed the coexistence of two particle populations. A population of smaller particles with hydrodynamic diameter of 1856 nm at peak maximum was present in larger volume % (Table 6). In addition, population of larger particles with the hydrodynamic radius around 5300 nm at peak maximum was observed. The order of magnitude greater hydrodynamic diameters (Table 6) than the sizes of spherical particles obtained from TEM micrographs (Table 5) indicates that measured hydrodynamic diameters corresponds to spherical particles chain-like aggregates. It seems that percentage of nonaggregated spherical ACP particles in the control systems is too low to be detected by DLS. The volume size distribution was broad, which is typical for this kind of systems.[30] ζ potential measurements showed that particles in control system after 10 min reaction time bear overall slightly negative charge ($\zeta = -2.7 \pm 0.7$ mV).

Table 5. Average diameter (*d*), its standard deviation (SD), corresponding minimum (min) and maximum (max) values of the spherical particles formed in the systems without and in the presence of monomer and micellar concentrations of DTAB and 12-2-12 after 10 and 30 minutes reaction time measured from transmission electron microscope (TEM) micrographs. $pH_{init} = 7.4$, θ / °C = (25 ±0.1).

t	**10 min**				**30 min**			
system	***d* / nm**	**SD**	**min**	**max**	***d* / nm**	**SD**	**min**	**max**
CS	127.0	55.8	18.3	282.2	55.5	10.9	37.6	82.9
MS1	151.2	44.1	51.6	294.2	73.8	13.5	44.3	109.9
MS2	67.5	26.8	30.0	156.6	49.9	16.9	21.2	112.9
DS1	83.0	18.6	36.3	140.1				
DS2	150.1	31.3	56.4	222.9				
DS3	149.4	45.5	75.1	225.9				

Control system (CS), DTAB monomers (MS1), DTAB micelles (MS2), 12-2-12 monomers (DS1), 12-2-12 spherical (DS2) and 12-2-12 elongated micelles (DS3)

In general, the dominant mechanism in formation of ACP is aggregation. Calcium and phosphate ions associate forming PNCs, which aggregate to spherical ACP particles, which in turn aggregate to chain-like aggregates.[6,9,10,29] Therefore, the processes that occur at the solution/precipitate interface are of utmost importance for the stability of ACP. This was, recently confirmed in the studies of ACP stabilization by citrate and magnesium ions, in which it was shown that the surface adsorbed ions, and not incorporated ones, play a decisive role.[36,42] Main driving forces in adsorption of the additive molecule on the precipitate/solution interface can range from purely electrostatic to highly specific recognition of crystal faces by the additive.[20,33] Adsorption behavior of simple additives is generally uncomplicated and can

be modeled accurately on the basis of the interactions between the adsorbing species and the surface of the substrate.[34] Surfactants adsorption behavior differs very much from that of small molecules due to their amphiphilic nature. At low surfactant concentrations, electrostatic interactions have a dominant role in the adsorption of ionic surfactants on the charged crystal faces (charged solids in general). As a result, surfactant monomers adsorb with their headgroups facing towards the substrate. With increasing concentration, as a consequence of hydrophobic interaction between surfactant tails, surfactant molecules tend to form aggregates at the solid/liquid interface, so called hemi-micelles.[34,35] This process is similar to the formation of the surfactant aggregates in the solution. Hydrophobic interactions become major driving force of adsorption at concentrations when the crystal surface becomes electrically neutral due to the adsorption. At concentrations above the cmc, surfactants adsorb with the headgroups facing towards the solution and a bilayer is formed. When maximum adsorption density is reached, increase in the surfactant concentration contributes only to the micellization in the solution.[34,35] In addition, the micelles formed in solution can be adsorbed directly on the substrate surface.[34]

As in control system, after 10 minutes reaction time in all precipitation systems containing DTAB (Fig. 2b,c and 3b,c) and 12-2-12 surfactant (Fig. 2d-e and 3d-e), PNCs, spherical ACP particles and their chain-like aggregates were formed. Therefore, the effect that surfactants exerted at these three length scales will be discussed.

The difference in effect that DTAB and 12-2-12 exhibited on properties of amorphous phase was observed already at monomer concentrations. While in the presence of DTAB monomers (MS1) smaller PNCs and larger spherical particles compared to control system were obtained, only size of spherical particles was affected by presence of 12-2-12 monomers (DS1). However, monomers of both surfactants had negligible effect on the size of chain-like aggregates (Table 6), although the percentage of lager aggregates was reduced in both cases. The difference in the behavior of DTAB and 12-2-12 monomers at nano scale could be a consequence of their different adsorption behavior due to the difference in their molecular structure and geometry. Based on the studies of DTAB and 12-2-12 adsorption at different substrates,[22,34] it is unexpected that DTAB monomers exhibited stronger effect on PNCs than 12-2-12 monomers. The great affinity of 12-2-12 monomers to adsorb on solid surfaces was also affirmed on AFM micrograph of DS1 system (Fig. 2d). A featureless bilayer typical for 12-2-12[34] was observed on mica, despite sample washing. These observations indicate that geometrical factor has an important role in surfactant molecules adsorption on ACP particles of different size. Due to the different molecular structure, DTAB and 12-2-12 molecules

19

occupy different minimum area at the solid/solution interface. The values of minimum area that molecules of these two surfactants occupy at the air/solution interface (Table 1) point that 12-2-12 as a result of additional headgroup and dodecyl chain in its molecular structure will occupy larger surface area than DTAB at the ACP/solution interface as well. In addition, the rigidity of ethylene spacer in the 12-2-12 molecule prevents it from enveloping around small PNCs when adsorbing. Therefore, DTAB molecules can be more easily accommodated at the solid ACP/solution interface preventing further grow of nanosized clusters. In addition, the effect of DTAB monomers on PNCs could have been more pronounced because they were present in much higher concentration ($c = 1 \cdot 10^{-4}$ mol dm^{-3}) than 12-2-12 ($c = 1 \cdot 10^{-5}$ mol dm^{-3}).

Since spherical particles are much larger than PNCs, the 12-2-12 molecules are more easily accommodated at the ACP/solution interface and difference in DTAB and 12-2-12 adsorption efficiency becomes more pronounced. ζ potential of the ACP particles obtained in the presence of DTAB monomers ($\zeta = 4.6 \pm 1.4$ mV) was slightly more positive than of the particles formed in the presence of 12-2-12 monomers ($\zeta = -0.7 \pm 0.2$ mV). At low surfactant concentration, adsorption on the solid surface is due to the electrostatic interactions between ions in the solid phase and ionic headgroups of the surfactants. This head on adsorption on solid surfaces results in the hydrophobic tails of surfactants protruding into the solution.[34,35] Considering that 12-2-12 molecule contains two charged headgroups and two alkyl chains and DTAB only one, more pronounced steric stabilization of ACP particles could be achieved by the adsorption of 12-2-12. This prevents growth of ACP spherical particles in DS1 system, but not in MS1. Previous studies have shown that in the presence of different additives *e.g.* magnesium ions and amino acids,[43] phosphorylated osteopontin peptides[38] and PEs[10], the size of ACP spherical particles is reduced.

DTAB and 12-2-12 micelles exhibited different effects of different length scales. While sizes of PNCs, obtained by AFM, in the presence of spherical DTAB (MS2) and 12-2-12 micelles (DS2) were not significantly different from the ones in control system, the clusters obtained in the presence of elongated 12-2-12 micelles (DS3) were larger (Table 4). In addition, height minimum and maximum values were also higher. The micelles formed in these systems do not differ only in charge density and distribution, but also in curvature. Elongated 12-2-12 micelles (DS3), which had most pronounced effect, have the lowest curvature. It was found that the Langmuir monolayer of arachidic acid promotes further aggregation and growth of PNCs in SBF.[13] These findings point to the conclusion that the
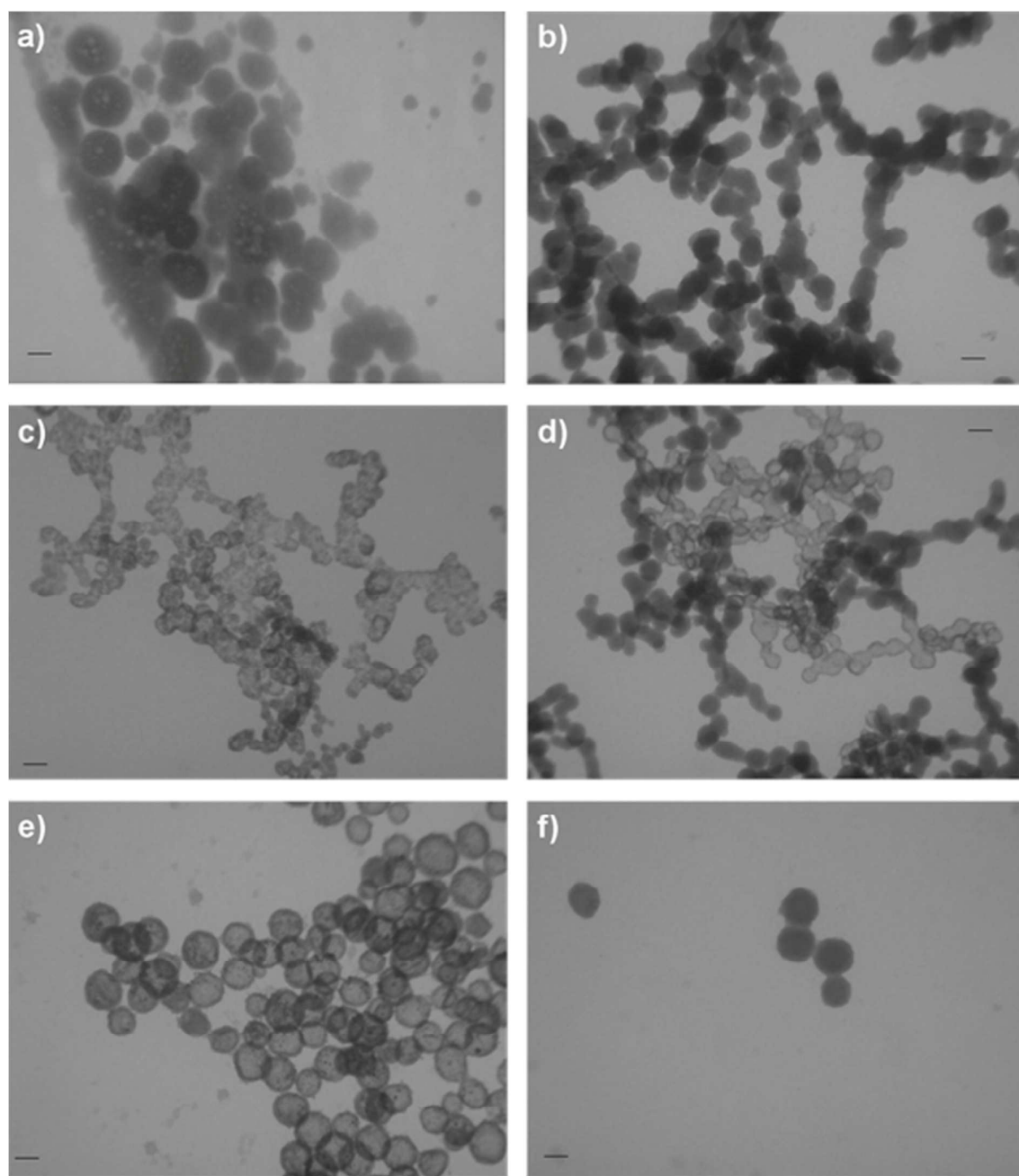
Figure 3. Transmission electron microscope (TEM) micrographs of the particles formed in the systems a) without (CS) and (b-f) in the presence of surfactants: b) DTAB monomers (MS1), c) DTAB micelles (MS2), d) 12-2-12 monomers (DS1), e) 12-2-12 spherical (DS2) and f) 12-2-12 elongated micelles (DS3) after 10 minutes aging time. $pH_{init} = 7.4$, θ / °C = (25 ±0.1). Bar = 100 nm.

templates of lower curvature promote aggregation of PNCs, most probably due to the fact that surface of lower curvature enables better contact between clusters.

Micelles exhibited pronounced effect on morphology and size of spherical ACP particles. The smallest spherical ACP particles were obtained in the presence of DTAB micelles. In addition, their appearance (Fig 3c), was different from the well delimited particles formed in other investigated systems. On the other hand, in the presence of 12-2-12 micelles (DS2 and DS3) spherical ACP particles, larger than in control and MS2 system, were detected after 10 min aging time (Fig. 3e,f, Table 5). In addition, in the presence of spherical 12-2-12 micelles (DS2) an interesting morphology was observed. Obtained spherical particles were similar to the hollow ACP spheres found in the microemulsions containing anionic asymmetric double-chained bis(2-ethylhexyl)sulfosuccinate (AOT).[49] Both 12-2-12 and AOT contain two alkyl chains, confirming that hydrophobic interactions have major role in determining final ACP morphology. Observed difference in size and morphology of ACP spherical particles formed in the presence of DTAB and 12-2-12 micelles demonstrate how chaining micelle properties, charge density and distribution, as well as curvature, could be used for achieving different effects in precipitation process.

Table 6. Average hydrodynamic diameter (d_h) with standard deviations (SD) and mean volume % of particles formed in the systems without and in the presence of monomer and micellar concentrations of DTAB and 12-2-12 after 10 minutes reaction time measured by dynamic light scattering. $pH_{init} = 7.4$, θ / °C = (25 ±0.1).

	Peak I			Peak II		
system	d_h / nm	SD	Mean vol %	d / nm	SD	Mean vol %
CS	1855.7	148.1	69.4	5272.0	686.0	30.6
MS1	1889.0	166.5	92.3	5097.7	103.0	7.7
MS2	1346.3	281.6	99.3	5312.0	147.1	0.7
DS1	1854.7	259.6	96.9	5243.0	302.6	3.1
DS2	1541.0	319.5	83.3	4855.3	732.8	16.7
DS3	205.1	14.25	100			

Control system (CS), DTAB monomers (MS1), DTAB micelles (MS2), 12-2-12 monomers (DS1), 12-2-12 spherical (DS2) and 12-2-12 elongated micelles (DS3)

Unlike monomers, both DTAB and 12-2-12 micelles exhibited pronounced effect on chain-like aggregates. In the presence of spherical DTAB (MS2) and 12-2-12 micelles (DS2), the value of the major peak maximum was shifted towards lower values and the percentage of larger particles was reduced, as compared to control system and systems containing surfactant monomers. Contrary to other investigated systems, at higher micellar 12-2-12 concentration,

at which elongated micelles were present (DS3), a monomodal size distribution was observed. In addition, notably smaller particles hydrodynamic diameter ($d_h \sim 205.1$ nm) was measured in DS3 system, indicating that elongated 12-2-12 micelles are the most efficient in preventing aggregation of spherical ACP particles. The fact that the most pronounced effect on aggregation processes was observed in the presence of elongated 12-2-12 micelles (DS3) indicate that, in addition to concentration, the curvature of the aggregate has considerable influence, as mentioned before.

Precipitation systems after 30 min reaction time. The presence of DTAB and 12-2-12 monomers and micelles in the precipitation systems affected kinetics and pathway of ACP transformation in different ways, as can be seen from pH *vs.* time curves (Fig. 1). As a consequence, after 30 min reaction time the precipitation process was at different stages in different investigated systems. In the control system and system containing monomer DTAB concentration (MS1) precipitation process was still in stage 2a (Fig. 1), *i.e.* transformation of ACP has not yet begun. Contrary to this, in the system with lower micellar 12-2-12 concentration (DS2) ACP/crystalline transformation has already begun (stage 3, Fig. 1), confirmed also by splitting of υ_4 PO4 band in FTIR spectra of formed precipitate (Fig. S5†). In all other precipitation systems after 30 minutes reaction time a change of precipitate morphology was observed. AFM and TEM micrographs of the precipitates formed in investigated systems after 30 minutes are shown in Figs. 4 and 5, respectively.

In the control system, size of PNCs and spherical particles decreased with aging time (Fig. 4a and 5a, Tables 4 and 5). It is known that the calcium carbonate clusters are present even after nucleation, *i.e.* at later stages of precipitation process.[48] The study of calcium carbonate nucleation has shown that long-lived precrital clusters grow by colliding and coalescing,[50] so if carbonate clusters are stable with respect to the solution state, they would grow larger.[14] The same conclusion could be drawn for PNCs. Analysis of AFM micrographs showed that in the control system average height of the PNCs, as well as maximum observed height, decreased after 30 min reaction time. The decrease in size indicates that PNCs in control system were not stable with respect to the solution. The size of spherical ACP particles as well as their chain like aggregates also decreased with time. DLS measurements of the chain-like ACP particles showed the existence of only one population of chain-like particles with the peak maximum at 1792 nm (Table 7). Second, *i.e.* larger, population of aggregated particles was not detected as opposed to the results obtained after 10 min.

Although the shape of pH curves suggest that ACP transformation in CS and MS1 systems proceeds via same pathway, the properties of ACP particles changed somewhat

23

differently than in control system. Contrary to the control system, at monomer DTAB concentration (MS1) the average size of PNCs remained unchanged after 30 minutes aging time. However, as in control system the sizes of spherical particles decreased compared to the particles formed after 10 min in the same systems (Fig. 5b, Table 5). On the other hand, in MS1 system bimodal distribution of chain-like aggregates of spherical particles was observed as after 10 min (Table 7). However, the values of peak maxima were shifted towards lower values.
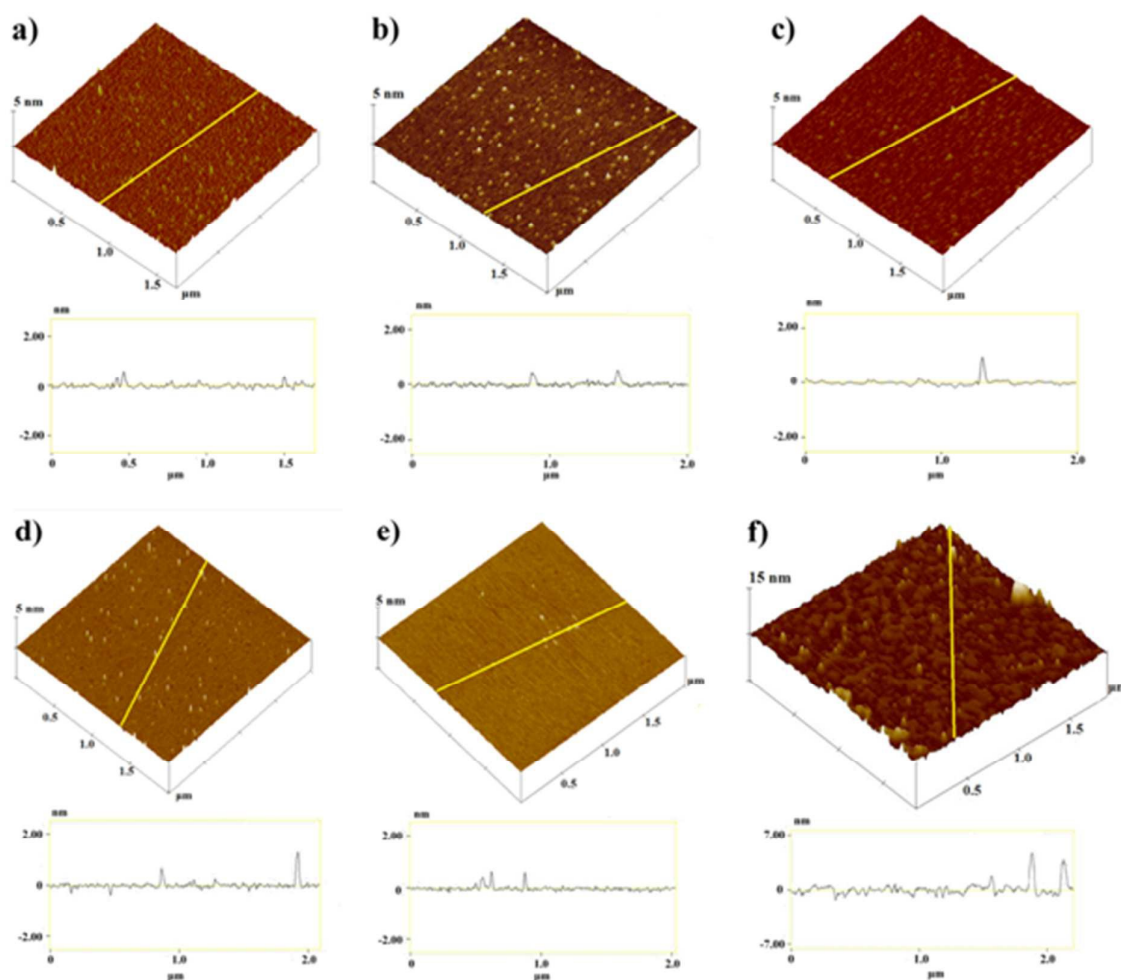
Figure 4. Atomic force microscopy 3D topographic views (top) and section profiles (bottom) of the particles formed in the systems a) without (CS) and (b-f) in the presence of surfactants: b) DTAB monomers (MS1), c) DTAB micelles (MS2), d) 12-2-12 monomers (DS1), e) 12-2-12 spherical (DS2) and f) 12-2-12 elongated micelles (DS3) after 30 minutes aging time. pH_{init} = 7.4, θ / °C = (25 ±0.1). All samples are presented on 2μm × 2 μm surface areas with vertical scales 5 nm (from a-e) and 15 nm (f).

In the presence of 12-2-12 change in ACP morphology was observed. As in the control system, the average height of the PNCs, as well as maximum observed height, decreased after 30 min aging time. The decrease in size indicates that PNCs, as in control system, were not stable with respect to the solution. As was pointed in discussion of the PNCs sizes obtained after 10 min reaction time, the tendency of 12-2-12 to adsorb at various interfaces is known. However, due to the small sizes of PNCs and molecular structure of 12-2-12, adsorption of dimeric surfactant was geometrically constrained. Therefore PNCs were not stabilized by 12-2-12 monomers. TEM micrographs revealed coexistence a small amount of ACP spherical particles and dense precipitate. DLS measurements reflected ongoing change of morphology. Obtained volume size distribution revealed coexistence of two particles population (Table 7, Figure S13†). The value of peak maximum of smaller particles was shifted toward larger value, while the volume percentage of larger particles increased, as compared to the results obtained after 10 min (Tables 6 and 7), confirming observed change.

After 30 minutes aging time, changes of ACP morphology were also detected in the presence of spherical DTAB (MS2) and elongated 12-2-12 micelles (DS3). In these systems a significant increase in the average size of the clusters, as well as height minimum and maximum value, was observed after 30 min aging time. The increase of PNCs sizes in the presence of micellar concentration of both surfactants indicates that surfactant micelles stabilized of PNCs even after longer aging time. In the presence of micellar DTAB concentration (MS2), a denser phase, with a morphology different from the one formed in DS1, was observed (Fig. 5c) in addition to spherical ACP particles. Similar dense phase was observed by Xie *et al.*[51] who proposed that it is ACP-II formed by partial dehydratation of ACP-I. Size analysis of spherical particles showed the reduction of their sizes as compared to the particles formed after 10 min in the same system. However, DLS results for particles at larger length scale showed opposite trend (Table 7, Figure S13c†). The volume size distribution obtained in the presence of spherical DTAB micelles (MS2) showed existence of two particles population, as after 10 min, with corresponding peak maxima shifted to higher values. In the presence of elongated 12-2-12 micelles (DS2) floccular precipitate and small amount of spherical particles was observed. The volume size distribution of particles obtained in the presence of higher micellar 12-2-12 concentration (DS3) remained monomodal, but the peak maximum value increased.
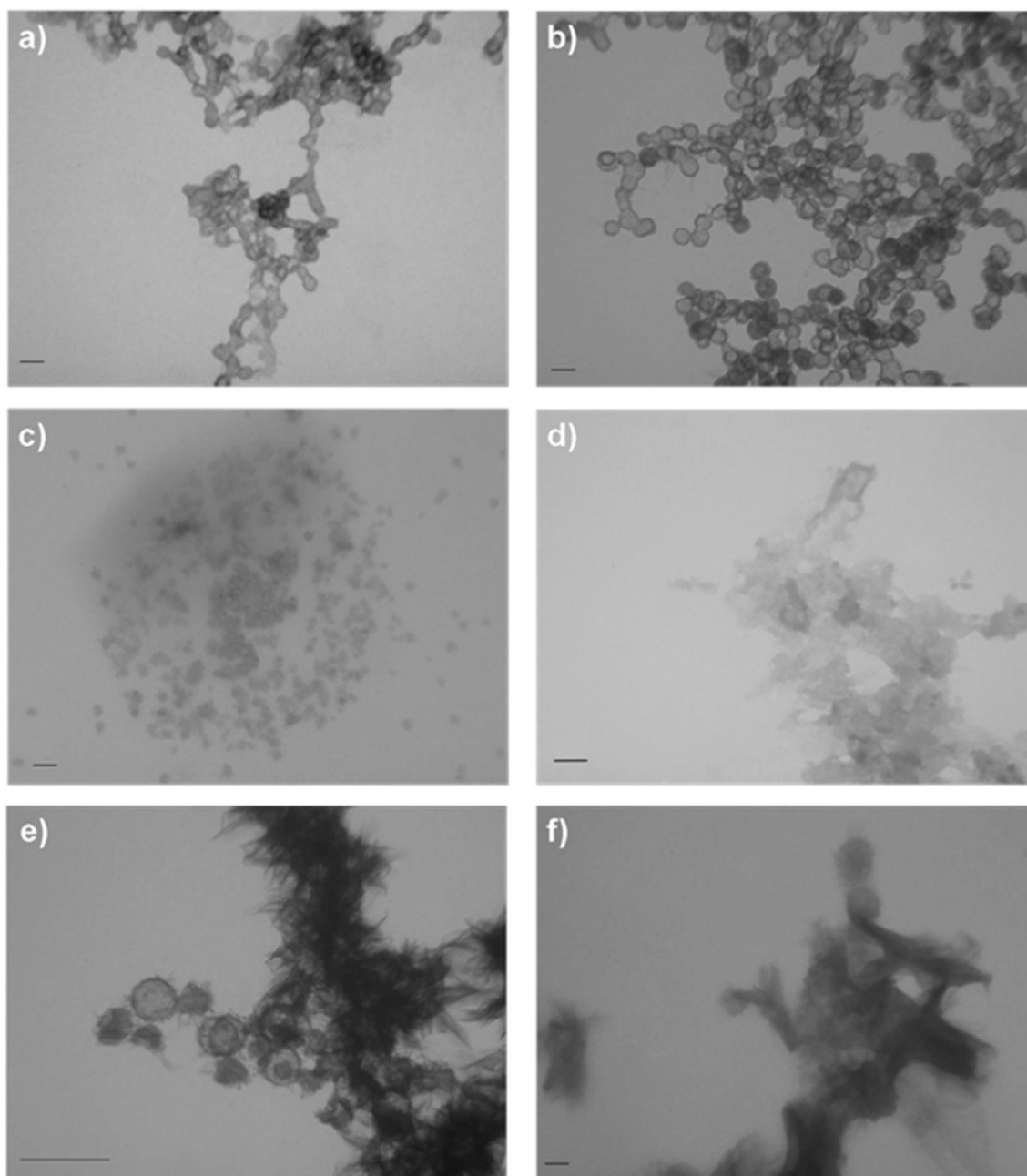
Figure 5. Transmission electron microscope (TEM) micrographs of the particles formed in the systems a) without (CS) and (b-f) in the presence of surfactants: b) DTAB monomers (MS1), c) DTAB micelles (MS2), d) 12-2-12 monomers (DS1), e) 12-2-12 spherical (DS2) and f) 12-2-12 elongated micelles (DS3) after 30 minutes aging time. pH_{init} = 7.4, θ / °C = (25 ±0.1). Bar = 100 nm

Although, the ACP transformation to crystalline phase has commenced after 30 minutes in DS2 system, PNCs were still detected. As in case of MS2 and DS3 systems, a significant increase in the size of the clusters was observed. TEM micrographs revealed that along a small percentage of spherical ACP particles, a sheet-like precipitate was formed confirming that the ACP/crystalline transformation has progressed the most in DS2 system. Splitting of v_4 phosphate band in FTIR spectra confirmed increased crystallinity of the precipitate (Fig. S14†). Similar results were reported by Ding *et al.*,[36] who observed the coexistence of spherical ACP particles and sheet-like HAP crystallites at the onset of the rapid pH drop (stage 3, Fig. 1), as well as at latter precipitation stages. Obtained volume size distributions in system containing 12-2-12 spherical micelles revealed coexistence of two particles population (Table 7). The value of peak maximum of smaller particles was shifted toward larger value, while the volume percentage of larger particles increased, as compared to the results obtained after 10 min (Tables 6).

Table 7 Average hydrodynamic diameter (d_h) with standard deviations (SD) and mean volume % of particles formed in the systems without and in presence of monomer and micellar concentrations of DTAB and 12-2-12 after 30 minutes reaction time measured by dynamic light scattering pH$_{init}$ = 7.4, θ / °C = (25 ±0.1).

t			30 min			
	Peak I			Peak II		
system	d_h / nm	SD	Mean vol %	d / nm	SD	Mean vol %
CS	1792.5	521.1	100			
MS1	1405.0	82.0	50.9	4363.0	148.5	49.1
MS2	1568.0	209.3	98.6	5443.5	43.1	1.4
DS1	2183.3	154.9	91.7	5216.0	272.9	8.3
DS2	2490.3	463.7	69.5	4147.0	113.1	30.5
DS3	514.7 ±	20.4	100			

Control system (CS), DTAB monomers (MS1), DTAB micelles (MS2), 12-2-12 monomers (DS1), 12-2-12 spherical (DS2) and 12-2-12 elongated micelles (DS3)

In summary, different effects of monomers and micelles of DTAB and 12-2-12 surfactants on properties of ACP was observed at different aging time and different length scales. In control system and in the presence of DTAB monomers (MS1) ACP transformation was direct. Contrary, in the presence of DTAB micelles (MS2), 12-2-12 monomer (DS1) and elongated micelles (DS3), change in morphology of precipitate was observed. In addition, morphology of precipitate was different in each system, indicating that interactions of surfactants with ACP were not the same in different systems. These diverse effects on ACP

27

transformation can be ascribed to the difference in surfactants molecular structure and their aggregation state. In addition to difference in charge density and distribution, rigidity of the headgroup and curvature of the aggregates should be taken into account. Interestingly, it seems likely that the additives effect on precipitation process observed at microscale could be a result of different pathways at nanoscale.

The influence of monomeric and dimeric surfactant on the properties of crystalline phase.

Precipitation systems after 24 h aging time. FTIR spectra, XRD patterns and TEM micrographs, (Figs. 6, 7, 8) of the precipitates formed in investigated systems revealed that in all systems ACP transformation was completed after 24 h reaction time. Detailed assignation of FTIR spectra is given in Table 8.

Similar to PEs,[10] surfactanats didn't have influence on composition of the formed precipitates. All FTIR spectra contained bands characteristic for OCP and apatitic phase (Fig. 6, Table 8). In the spectra of the precipitates obtained in micellar DTAB (MS2) and 12-2-12 solutions (DS2, DS3) bands of asymmetric and symmetric stretching of DTAB CH_2 and 12-2-12 C-H groups were observed, respectively (Fig. 6 c, e, f). Considering that the precipitates were thoroughly washed, this finding indicates that surfactants were tightly bound. In the case of 12-2-12, intensity of the bands increased with 12-2-12 concentration, indicating its progressive incorporation in the precipitate. XRD patterns (Fig. 7) revealed that in addition to OCP and HAP in all investigated systems, DCPD was formed (due to the small amount of precipitate formed in MS2 system, not all OCP and HAP reflections observed in patterns of other systems are present). Considering that no characteristic DCPD bands could be discerned in FTIR spectra and that only most intensive reflection (020) is present in XRD patterns it could be assumed that amount of precipitated DCPD is small.

However, TEM micrographs showed that surfactants affected precipitate morphology. In the control system a heterogeneous mixture of small, thin, plate-like crystals and poorly crystalline sheet-like precipitate was formed, as visualized with TEM (Fig. 8a). Selected area electron diffraction (SAED) from the crystals showed pattern characteristic for OCP,[10] but diffuse ring characteristic for amorphous material was also observed (inset in Fig. 8a).

28
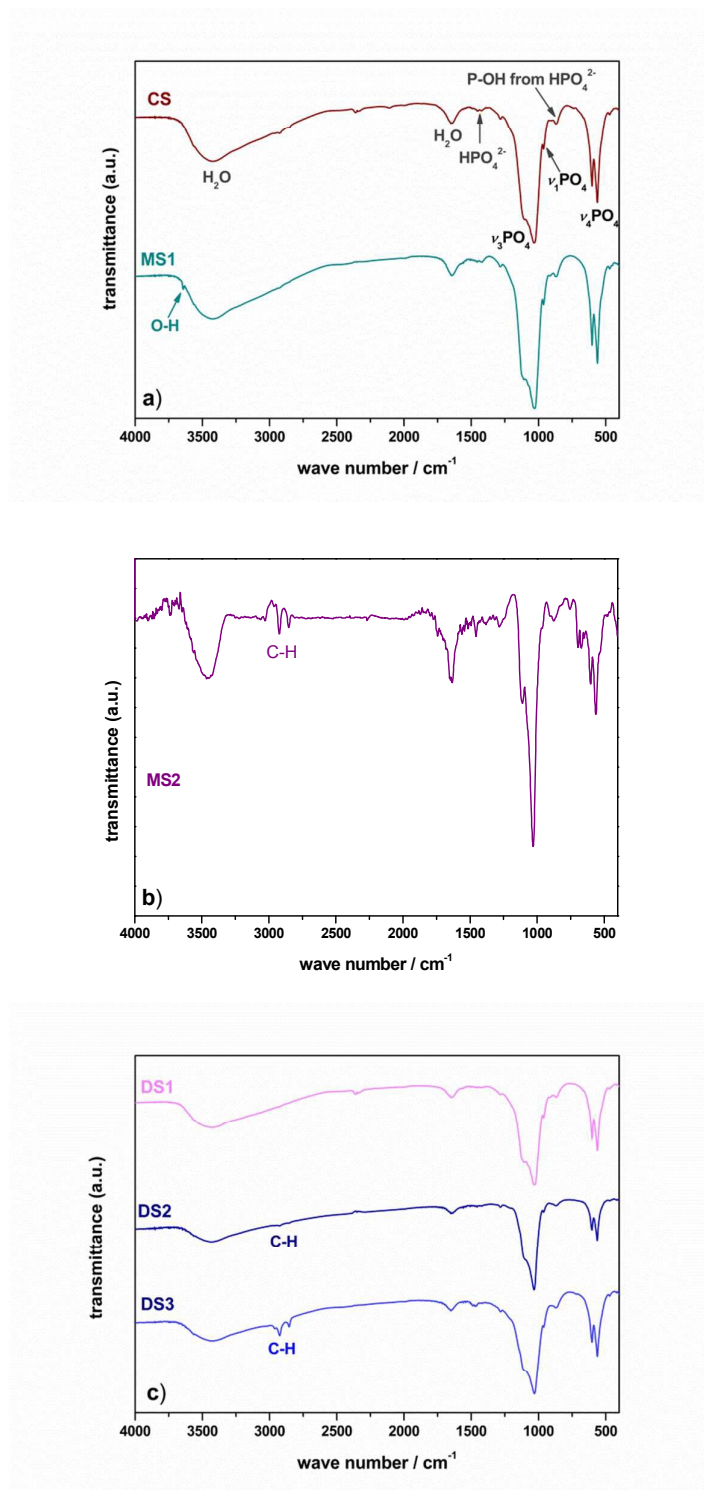
Fig. 6 Fourier transform infrared (FTIR) spectra of the precipitates formed in the control system (CS) and in the presence of monomer and micellar concentrations of DTAB and 12-2-12 after 24 h reaction time. $pH_{init} = 7.4$, $\theta / ^\circ C = (25 \pm 0.1)$. a) Control system (CS) and DTAB monomers (MS1), b) DTAB micelles (MS2), c) 12-2-12 monomers (DS1), 12-2-12 spherical (DS2) and 12-2-12 elongated micelles (DS3).

Table 8 Assigment of IR bands in FTIR spectra of precipitates formed in investigated systems after 24 hours. $pH_{init} = 7.4$, $\theta / °C = (25 \pm 0.1)$.

Wavenumber / cm^{-1}						Peak assignement	Ref.
CS	MS1	MS2	DS1	DS2	DS3		
3700–3000	3677-3000	3650-3300	3655-3055	3650-3200	3677-3100	Water vibration	52
	3645	3734				v_s stretching mode of O–H	52
				2970–2840	2970–2840	asymmetric and symmetric stretching of 12-2-12 C-H groups	53
		2919				asymmetric stretching of DTAB CH$_2$ groups	54
		2852				symmetric stretching of DTAB CH$_2$ groups	54
1643	1643	1635	1641	1641	1652	water vibration	52
					1488	v_3 stretching mode of CO_3^{2-} in CaP	52
1450	1467	1459			1459	v_3 or v_4 bending mode of CO_3^{2-}	52
1420	1423	1392				v_3 stretching mode of CO_3^{2-}	55
1281	1282	1284	1284	1284	1284	HPO_4^{2-} OH in plane bending	56
1113	1114	1114	1120	1109	1115	v_{3a} triply degenerate asymmetric stretching mode of PO_4^{3-} (P–O bond)	52
1028	1026	1030	1030	1029	1030	v_{3c} triply degenerate asymmetric stretching mode of PO_4^{3-} (P–O bond)	52
956	963	962	967	962	962	v_1 nondegenerate symmetric stretching mode of PO_4^{3-} (P–O bond)	52
870	867	872	865	866	866	HPO_4^{2-}	55
		752				v_4 in-plane deformation bending mode of CO_3^{2-} (O–C–O bond)	57
		695				v_4 in-plane deformation bending mode of CO_3^{2-} (O–C–O bond)	57
		645				v_L librational mode of OH (O–H bond)	52
600	602	605	600	605	600	v_{4a} triply degenerate bending mode of PO_4^{3-} (O–P–O bond)	52
561	561	560	560	560	560	v_{4b} triply degenerate bending mode of the PO_4^{3-} (O–P–O bond)	52
469	472	463	463		470	v_2 doubly degenerate bending mode of PO_4^{3-} (O–P–O bond)	52

Control system (CS), DTAB monomers (MS1), DTAB micelles (MS2), 12-2-12 monomers (DS1), 12-2-12 spherical (DS2) and 12-2-12 elongated micelles (DS3)

TEM images of the precipitates formed in the presence of DTAB (Fig. 8b, c) and 12-2-12 (Fig. 8d-f) show that monomers and micelles differently affected morphology of crystalline phase. In precipitation systems with DTAB and 12-2-12 monomers (MS1 and DS1) after 24 hours aging time a heterogeneous mixture of crystals and sheet-like precipitate was formed (Fig. 8b,d). However, contrary to the control system where only small OCP

30

crystals were formed, large, well developed, thin plate-like crystals were observed. These crystals have OCP structure, as confirmed with SAED (inset in Fig. 8b). In the case of precipitate formed in DS1 system, SAED pattern indicated the mixture of smaller and larger OCP crystals obtained in different orientations (Fig. 8d). However, no change in OCP morphology was observed compared to MS1 (Figs. 8b,d).

In the same experimental conditions, polyelectrolytes, PLL, PGA and PSS, also affected OCP crystal morphology.[10] In the presence of PEs, affected OCP crystals appeared smaller and thinner, with rounded edges. This nonspecific inhibition of crystal growth in all directions is due to the adsorption of the flexible PEs at all active sites.[10] An answer to a question why larger OCP crystals appeared in the presence of the DTAB and 12-2-12 monomers in such a complex system, where several CaP phases are simultaneously formed, is not straightforward. On the one hand it could mean that surfactant monomers promoted OCP crystal growth and the crystal grew larger. An example is growth of larger calcium oxalate monohydrate crystals (COM) in the presence of nefrocalcin isoforms with lower surface activity. However, these isoforms also promoted COM aggregation.[58] On the other hand, larger and more regular crystals can be obtained if nucleation rate is reduced, due to *e.g.* lowering the supersaturation.[59] Lower supersaturation with the respect to OCP could be achieved if DTAB and 12-2-12 monomers promote growth of other CaP phases.

Small, spherical DTAB micelles (MS2) didn't influence morphology of the CaP precipitate formed after 24 hours. Only a small amount of precipitate with morphology similar to the control system was formed (Fig. 8c). SAED shown in inset of Fig. 8c indicates that precipitate is poorly crystalline, since diffuse ring characteristic for amorphous material was observed. In addition, the rings characteristic for small crystals in different orientations were visible (rings observed in SAED pattern consists of low intensity spots).

In the presence of 12-2-12 micelles (DS2 and DS3) no large OCP crystals were observed. A sheet-like crystallites, were observed on TEM micrographs (Figs. 8e, f). Diffuse rings characteristic for amorphous material and nanocrystalls in different orientations were observed in SAED patterns (insets in Figs. 8e, f). A possible explanation of observed effect is nonspecific interaction of surfactant micelles with all growing faces of OCP crystals, which prevents formation of large well developed plate-like crystals.
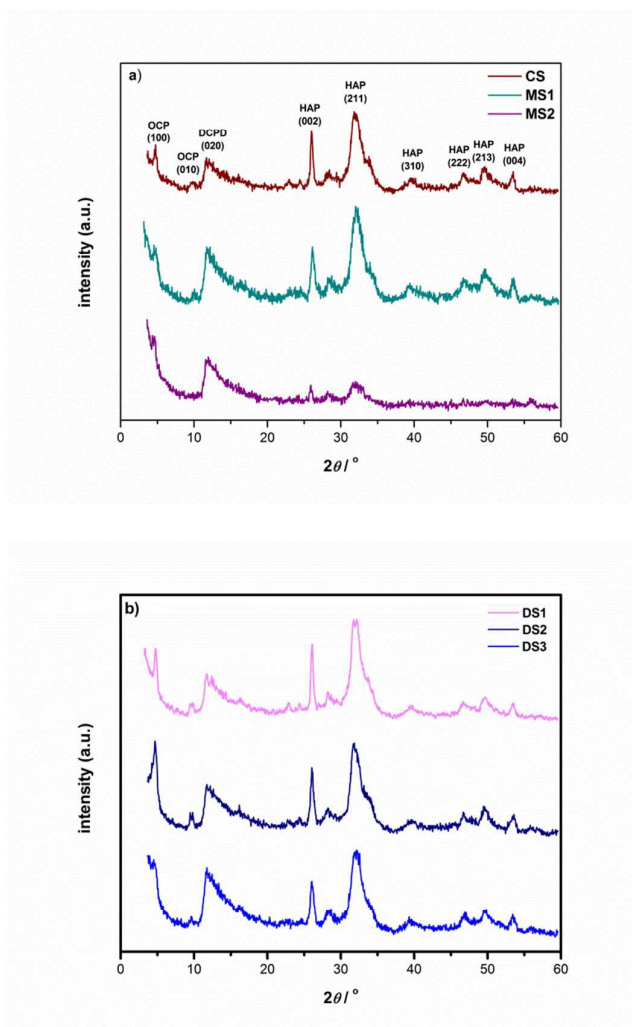
Fig. 7 XRD patterns of the precipitates formed in the control system (CS) and in the presence of monomer and micellar concentrations of DTAB and 12-2-12 after 24 h reaction time. pH_{init} = 7.4, θ / ° C = (25 ±0.1). a) Control system (CS), DTAB monomers (MS1) and DTAB micelles (MS2), b) 12-2-12 monomers (DS1), 12-2-12 spherical (DS2) and 12-2-12 elongated micelles (DS3).OCP, DCPD and HA diffractions are marked.

In summary, neither surfactant monomers nor micelles influenced composition of the precipitate. In all systems a mixture of OCP, HAP and DCPD was formed. However, surfactant molecular structure and aggregation state had decisive role in determining surfactants influence on morphology of crystalline phase, as well as on pathway of its formation (Scheme 2). In the presence of DTAB and 12-2-12 monomers OCP crystals larger than in control were observed. 12-2-12 monomers exhibited their influence on precipitate morphology in the earlier stage of precipitation process compared to DTAB monomers, most probably due to their higher tendency of adsorption. In the presence of both 12-2-12 spherical

32
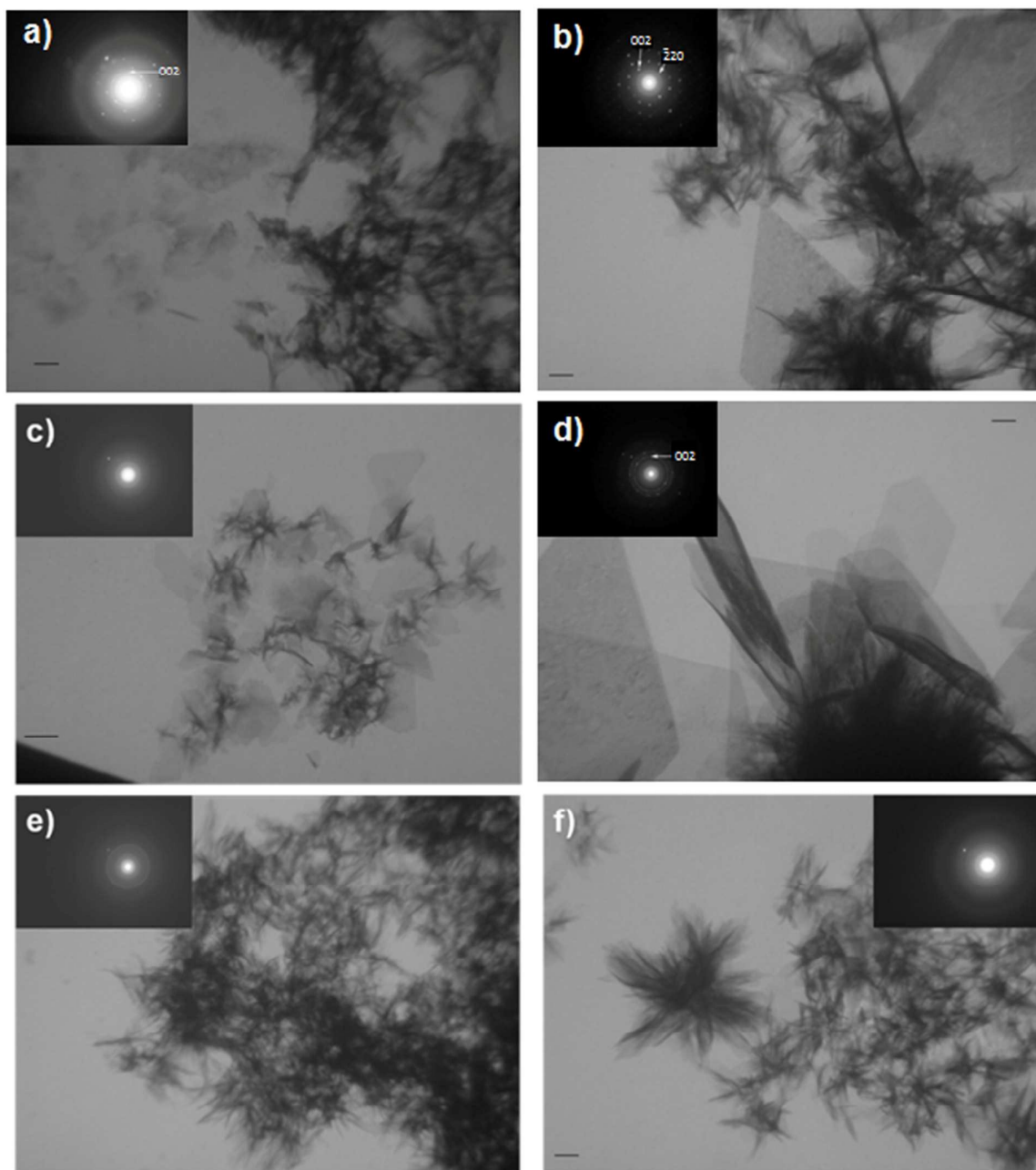
Figure 8. Transmission electron microscope (TEM) micrographs and corresponding selected area electron diffraction (SAED) patterns (insets in the figures) of the particles formed in the systems a) without (CS) and (b-f) in the presence of surfactants: b) DTAB monomers (MS1), c) DTAB micelles (MS2), d) 12-2-12 monomers (DS1), e) 12-2-12 spherical (DS2) and f) 12-2-12 elongated micelles (DS3) after 24 hours aging time. Bar = 100 nm.

33
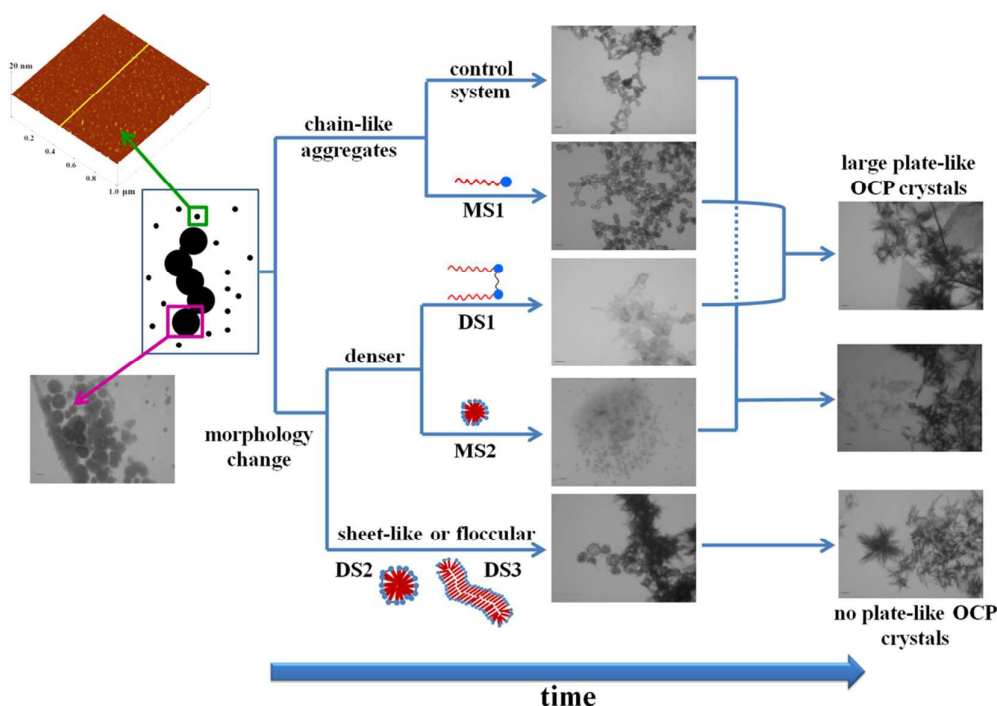
Scheme 2. Schematic representation of observed pathways of ACP/crystalline transformation in the control system and in the presence of monomeric and micellar concentrations of DTAB and 12-2-12. Micrographs are taken with atomic force and transmission electron microscopy. pH_{init} = 7.4, θ / ° C = (25 ±0.1). Control system (CS), DTAB monomers (MS1), DTAB micelles (MS2), 12-2-12 monomers (DS1), 12-2-12 spherical (DS2) and 12-2-12 elongated micelles (DS3).

(DS2) and elongated micelles (DS3) no plate-like OCP crystals were observed. On the other hand, in the presence of DTAB micelles small OCP crystals, similar to those obtained in control system, were formed. The difference in the effect on ACP formation and transformation between DTAB and 12-2-12 surfactants demonstrates how change in molecular structure can have profound impact on precipitation process although chemistry of the molecule was not changed. Chemically linking two DTAB molecules into 12-2-12 resulted in different charge density and flexibility of the molecules. As a consequence both adsorption and aggregation processes of DTAB and 12-2-12 monomers are greatly affected.[22] This results in diverse effects observed in the precipitation systems and points to the charge density and distribution, as well as geometry of the micelles as a principle factors responsible for the observed effects.

34

CONCLUSIONS

Combination of microscopy (AFM and TEM) and light scattering (DLS and ζ potential measurements) techniques, enabled to follow simultaneously the influence that DTAB and 12-2-12 monomers and micelles exhibit on the formation and transformation of ACP at different stages and at different length scales of precipitation process. Depending on their aggregation state (monomers or micelles) and the geometry of aggregate (spherical or elongated micelles) DTAB and 12-2-12 have exhibited different effects on the rate of ACP transformation, as well as on the properties of ACP and crystalline phase. The difference in monomers and micelles charge density and distribution, which is a consequence of their different molecular structure, as well as presence of geometrical constrain in 12-2-12 molecule, affects both the efficiency of their adsorption at different sized substrates and the templating ability of their micelles. Unlike small molecular additives, for which main driving forces in solid phase/additive interactions are electrostatic, for surfactants hydrophobic interactions play important role in addition to electrostatic interactions. Moreover, the surfactants effect on precipitation process observed at microscale could be a result of different pathways at nanoscale. Obtained results may have implications for understanding general mechanism of inorganic-organic interactions underlying biomineralization processes, as well as for materials science, especially for the control of materials preparation at nanoscale.

† Electronic supplementary information (ESI) available: details of surfactant/Na_2HPO_4 systems characterization, FTIR spectra of precipitates formed in the control and DS2 systemafter different aging timesd AFM images of large ACP particles and micelles; DLS measurements of PNCs and polymeric assemblies of nanoclustersd ACP particles size distributions obtained from AFM and TEM micrographs and DLS measurements.

References

1. S. Dorozhkin, *Calcium Orthophosphates. Application in Nature, Biology and Medicine*, Pan Stanford Publishing, Singapore, 2012

2. L. Wang and G.H. Nancollas, *Chem. Rev.*, 2008, **108**, 4628–4669.

3. J. Zhao, Y. Liu, W.-B. Sun and H. Zhang, *Chem. Cent. J.,* 2011, **5**, 40 DOI: 10.1002/jbm.a.10426

4. J. Mahamid, A. Sharir, L. Addadi and S.Weiner, *Proc. Natl. Acad. Sci. U.S.A.*, 2008, **105**, 12748-12753.

5. E. Beniash, R. A. Metzler, R. S. K. Lam and P. U. P. A. Gilbert, *J. Structural Biology*, 2009, **166**, 133-143.

6. C. Combes, and C. Rey, *Acta Biomater.*, 2010, **6**, 3362-3378.

7. E. D. Eans, I. H. Gillesen, and A. S. Posner, *Nature* (London), 1965, **208**, 365-367.

8. A. S. Posner and F. Betts, *Acc. Chem. Res.*, 1975, **8**, 273-281.

9. Lj. Brečević, V. Hlady and H. Füredi-Milhofer, *Colloids Surf.*, 1987, **28**, 301 – 313.

10. P. Bar-Yosef Ofir, R. Govrin-Lippman, N. Garti and H. Füredi-Milhofer, *Cryst. Growth Des.*, 2004, **4**, 177-183.

11. K. Onuma, and A. Ito, *Chem. Mater.*, 1998, **10**, 3346-3351.

12. A. Oyane, K. Onuma, T. Kokubo and A. Ito, *J. Phys. Chem. B*, 1999, **103**, 8230-8235.

13. A. Dey, P. H. H. Bomans, F. A. Müller, J. Will, P.M. Frederik, G. de With and N. A. J. M. Sommerdijk, *Nature Materials*, 2010, **9**, 1010-1014.

14. L. Wang, S. Li, E. Ruiz-Agudo, C. V. Putnis and A. Putnis, *CrystEngComm*, 2012, **14**, 6252-6256.

15. Lj. Brečević, and H. Füredi-Milhofer, *Calcif. Tissue. Res.*, 1972, **10**, 82-90.

16. R. Despotović, N. Filipović-Vinceković and H. Füredi-Milhofer, *Calcif. Tissue. Res.*, 1975, **18**, 13-26.

17. J. Christoffersen, M.R. Christoffersen, W. Kibalczyc and F.A. Andersen, *J. Cryst. Growth*, 1989, **94**, 767-777.

18. H. Pan, X.-Y. Liu, R. Tang and H.-Y. Xu, *ChemComm*, 2010, **46**, 7415-7417.

19. M. Iijima, D. Fan, K. M. Bromley, Z. Sun and J. Moradian-Oldak, *Cryst. Growth Des.*, 2010, **10**, 4815-4822.

20. M. Dutour Sikirić, and H. Füredi-Milhofer, *Adv. Colloid Interface Sci.*, 2006, **128**, 135–158.

21. M. Ramanathan, L. K. Shrestha, T. Mori, Q. Ji, J. P. Hill and K. Ariga, *Phys. Chem. Chem. Phys.*, 2013, **15**, 10580-10611.

22. R. Zana, *Adv. Colloid Interface Sci.*, 2002, **97**, 205-253.

23. M. Sikirić, I. Primožič, Y. Talmon and N. Filipović-Vinceković, *J. Colloid Interface Sci.*, 2005, **281**, 473-481.

24. D. Jurašin, I. Habuš and N. Filipović-Vinceković, *Colloids Surf. A*, 2010, **368**, 119-128.

25. J. Xia and R. Zana, in *Gemini Surfactants, Synthesis, Interfacial and Solution – Phase Behaviour and Applications*, ed. R. Zana and J. Xia, Marcel Dekker, New York, 2004, Chapter 13, 296-315.

26. D. Danino, Y. Talmon and R. Zana, *Langmuir*, 1995, **11**, 1448-1456.

27. M. J. Rosen, *Surfactants and Interfacial Phenomena*, 3rd Ed, Wiley Interscience: Hoboken, New Jersey, 2004.

28. J.R. de Bruyn, M. Goiko, M. Mozaffari, D. Bator., R. L. Dauphinee, Y. Liao, R. L. Flemming, M. S. Bramble, G. K. Hunter and H. A. Goldberg, *PLOS ONE*, 2013, **8**, e56764 (DOI 10.1371/journal.pone.0056764).

29. X. Yang, L. Wang, Y. Qin, Z. Sun, Z. J. Henneman,; J. Moradian-Oldak and G. H. Nancollas, *J. Phys. Chem. B*, 2010, **114**, 2293-2300.

30. C.-G. Wang, J.-W. Liao, B.-D. Gou, J. Huang, R.-K. Tang, J.-H. Tao, T.-L. Zhang and K. Wang, *Cryst. Growth Des.*, 2009, **9**, 2620-2626.

31. C.K. Liu and G. Warr, *Langmuir*, 2012, **28**, 11007-11016.

32. M. Pisárčik, M. Dubničková, F. Devínsky, I. Lacko and J. Škvarla, *Colloids Surf. A*, 1998,**143**, 69–75.

33. K. Bleek, and A. Taubert, *Acta Biomater.*, 2013, **9**, 6283-6762.

34. R. Atkin, V. S. J. Craig, E. J. Wanless and S. Biggs, *Adv. Colloid Interface Sci.,* 2003, **103**, 219-304.

35. R. Zhang and P. Somasundaran, *Adv. Colloid Interface Sci.*, 2006, **123-126**, 213-229.

36. H. Ding, H. Pan, X. Xu and R. Tang, *Cryst. Growth Des.*, 2014, **14**, 763–769.

37. *CRC Handbook of Chemistry and Physics*, ed. D. R. Lide,CRC Press, Boca Raton, 2004.

38. S. Li and L. Wang, *CrysEngComm*, 2012, **14**, 8037-8043.

39. J. Yao, W. Tjandra, Y.Z. Chen, K.C. Tam, J. Ma and B. Soh, *J. Mater. Chem.*, 2003, **13**, 3053-3057.

40. W. J. E. M. Habraken, J. Tao, L. J. Brylka, H. Friedrich, L. Bertinetti, A. S. Schenk, A. Verch, V. Dmitrovic, P. H. H. Bomans, P. M. Frederik, J. Laven, P. van der

Schoot, B. Aichmayer, G. de With, J. J. DeYoreo and N. A. J. M. Sommerdijk, *Nature Communications*, 2013, **4**, 1507.

41. S. Jiang, Y. Chen, H. Pan, Y.-J. Zhang, R. Tang, *Phys. Chem. Chem. Phys.*, 2013, **15**, 12530

42. Y. Chen, W. Gu, H. Pan, S. Jiang and R. Tang, *CrystEngComm*, 2014, **16**, 1864-1867.

43. X. Yang, B. Xie, L. Wang, Y. Qin, Z.J. Henneman and G. H. Nancollas, *CrystEngComm*, 2011, **13**, 1153-1158.

44. A.Bigi, E. Boanini, G. Cojazzi, G. Falini and S. Panzavolta, *Cryst. Growth Des.*, 2001, **1**, 239-244.

45. R. F. Domingos, M. A. Baalousha, Y. Ju-Nam, M. M. Reid, N. Tufenkji, J. R. Lead, G. G. Leppard and K. J. Wilkinson, *Environ. Sci. Technol*,. 2009, **43***, 7277–7284.

46. H. Kato, in *Nanomaterials: Processing and Characterization with Lasers*, ed. S. C. Singh, H. Zeng, C. Guo and W. Cai, Wiley-VCH Verlag GmbH & Co. KGaA, Weinheim, 2012, Chapter 8, 535-554.

47. D. Gebauer, M. Kellermeier, J. D. Gale, L. Bergström and H. Cölfen, *Chem. Soc. Rev.*, 2014, **43**, 2348-2371.

48. E. M. Pouget, P. H. H. Bormans, J. A. C. M. Goos, P. M. Frederik, G. de With and N. A. J. M. Sommerdijk, *Science*, 2009, **323**, 1455-1458.

49. C. E. Fowler, M. Li, S. Mann and H. C. Margolis, *J. Mat. Chem*., 2005, **15**, 3317-3325.

50. D. Gebauer, A. Völkel and H. Cölfen, *Science*, 2008, **322**, 1819–1822.

51. B. Xie, T. J. Halter, B. M. Borah and G. H. Nancollas, *Cryst. Growth Des.*, 2014, **14**, 1659–1665.

52. S. Koutsopulos, *J. Biomed. Mater. Res.*, 2002, **62**, 600-612.

53. B. Brycki, I. Kowalczyk and A. Kozirog, *Molecules*, 2011, **16**, 319-335.

54. R. B. Viana, A. B. F. Da Silva and A. S. Pimentel, *Adv. Phys. Chem.*, 2012, Article ID 903272.

55. C. Mochales, R. M. Wilson, S. E. P. Dowker and M.-P. Ginebra, *J.All.Com*., 2011, **509**, 7389-7394.

56. J. V. Rau, M. Fosca, V. S. Komlev, I. V. Fadeeva, V. R. Albertini and S. M. Barinov, *Cryst. Growth Des*., 2010, **10**, 3824-3834.

57. F. A. Andersen and Lj. Brečević, *Acta Chem. Scand*., 1995, **45**, 1018–1024.

58. J. W. Kurutz, M. Carcalho and Y. Nakagawa, *J. Cryst. Growth*, 2003, **255**, 392-402.

59. H. E. L. Madsen and J. B. Pedersen, in *Advances in Crystal growth Inhibition Technologies*, ed. Z. Amjad, Kluwer Academic Publisher, New York, 2002; Chapter 1, 1-15.